

RSC Advances



This is an *Accepted Manuscript*, which has been through the Royal Society of Chemistry peer review process and has been accepted for publication.

Accepted Manuscripts are published online shortly after acceptance, before technical editing, formatting and proof reading. Using this free service, authors can make their results available to the community, in citable form, before we publish the edited article. This *Accepted Manuscript* will be replaced by the edited, formatted and paginated article as soon as this is available.

You can find more information about *Accepted Manuscripts* in the [Information for Authors](#).

Please note that technical editing may introduce minor changes to the text and/or graphics, which may alter content. The journal's standard [Terms & Conditions](#) and the [Ethical guidelines](#) still apply. In no event shall the Royal Society of Chemistry be held responsible for any errors or omissions in this *Accepted Manuscript* or any consequences arising from the use of any information it contains.

Chemical-Mechanical Properties of Tribofilms and its Relation to Ionic Liquid Chemistry

Vibhu Sharma¹, Nicole Doerr², Pranesh B Aswath¹

¹Materials Science and Engineering Department University of Texas at Arlington,
Arlington, TX, USA

²AC²T research GmbH, Austria

Contact Author: Professor Pranesh B. Aswath, 001-817-272-0308, Aswath@uta.edu

ABSTRACT: The relationship between the ionic liquid (IL) chemistry to its tribological properties such as coefficient of friction, wear and chemical-mechanical properties of tribofilms is examined. In this study, six phosphorous (P) based IL's (in which P is either present in anion or in cation or in both) were chosen to examine the role of different cations and anions. The six IL's used as additives were blended in group I base oil at 0.1 wt. % P treat rate and their tribological performance was evaluated using a cylinder on reciprocating flat test configuration under pure sliding contact. ZDDP at 0.1 wt. % P and base oil tests were also conducted for baseline comparison. All IL's exhibited comparable or lower coefficient of friction compared to ZDDP that has a higher but consistent coefficient of friction for the duration of the test. IL N_DEHP and P_TFSI exhibited comparable or slightly better wear protection compared to ZDDP whereas N_DBDTP, P_TMPP, P_DMP and P_DEDTTP exhibited worse wear outcomes than ZDDP. XANES analysis of pure IL standards and their tribofilms indicate that the tribofilms from IL are the result of decomposition of the IL chemistry and reaction of these decomposition products with underlying steel substrate. No residues of the original IL chemistry was found on the wear tracks. Nano-indentation results indicated that tribofilm hardness increases from the surface towards the bulk of the films, which when combined with P L-edge spectra indicate that short chain phosphates formed at the surface result into lower hardness than medium chain phosphate formed in the bulk.

1. INTRODUCTION

The on-going trend in automotive industry is to improve their efficiency and fuel economy as well as increase their longevity and reliability while at the same time reduce the harmful emission to the environment. The efficiency of the automotive systems can be improved significantly by reducing the frictional losses as well as by minimizing the wear. In a recent study, Holmberg et al.^{1, 2} concluded that latest technological advances in the field of tribology could lead to up to 14% reduction in frictional losses in heavy duty vehicles and up to 18% friction reduction in passenger vehicles in short term (i.e. within 5-10 years). At the same time CO₂ emission could also be reduced by 200 million tonnes in heavy duty vehicles and 290 million tonnes in passenger vehicles. Potential technological advances in tribology include novel lubricant additives such as ionic liquids (IL's)³⁻⁸, ashless fluorothiophosphates⁹⁻¹², low friction coatings¹³, surface texturing¹⁴ and low viscosity and low shear lubricant oil's¹⁵.

Of all the approaches used, additive development offers the potential for providing in-situ low friction film formation at a low cost and our study focuses on oil soluble ionic liquids (IL's) that include phosphorous as one of the constituents. IL are well known compounds and have been used in many engineering applications¹⁶⁻²⁰. IL's in tribology is a relatively new development, with application of IL's as lubricant/lubricant additive first recognized in 2001²¹. The advantages of ionic liquids include their negligible vapor pressure, high thermal stability, non-flammability, non-volatility and electrochemical properties that are highly desirable for tribological applications. However, their limitations have included low solubility in oils due to their highly polar structure that can be mitigated to some extent by engineering their structure²².

Most IL's used in engineering applications are synthetic salts and depending on the choice of a cation and anion, can be made available in various structures. In tribology, only few specific structures can be used as lubricant and lubricant additives. Earlier studies on IL's as lubricant/lubricant additives focused on imidazolium based cation with tetrafluoroborate and hexafluorophosphate anions²³⁻²⁷. Jiménez et al.²³ studied 1-N-alkyl-3-methylimidazolium

based IL's with tetrafluoroborate and hexafluorophosphate anions as neat lubricant and lubricant additives and reported a significant improvement in lubrication properties (friction and wear reduction) when IL's are added in base oil as an additives (1 wt%) in comparison to when used as neat lubricants at room temperature as well at 100 °C. In another study by Jiménez et al.²⁸, lubrication properties of imidazolium based IL's were studied at low as well as at elevated temperatures. They reported that tetrafluoroborate 1-hexyl/octyl-3-methylimidazolium IL's show higher thermal stability and better lubricating performance than mineral and synthetic oils under extreme temperature conditions, both at low (-30 °C) and high (100 °C, 200 °C) temperatures. Tribocorrosion due to IL's was also observed in the case of more polar and shorter alkyl chain tetrafluoroborate 1-hexyl-3-methylimidazolium IL at elevated temperature. Pisarova et al.²⁹ studied the thermal stability and corrosion properties of ammonium based IL's with Bis (trifluoromethylsulfonyl) imide (NTF₂) and methanesulfonate anions. They reported that corrosiveness of IL's depends on the choice of cation and anion, choline NTF₂ IL showed significantly lower corrosiveness and higher thermal stability than choline methanesulfonate IL. Pisarova et al.³⁰ also studied the degradation mechanism of ammonium IL's and their tribological properties using mass spectrometry. An intermolecular transmethylation in ammonium IL was identified under long term thermo-oxidative stress. They also suggested that IL altered products due to thermal degradation can negatively influence their tribological performances. Imidazolium and ammonium based IL's with halogenated anions (PF₆⁻, BF₄⁻ and Bis trifluorosulfonyl imide TFSI⁻) show potential improvement in friction and wear performance when used as neat lubricant or as lubricant additive in base oil. However, corrosiveness and solubility in non-polar base oil is still a limitations to their tribological application. Totolin et al.³¹ studied and compared the tribological properties of halogenated and halogen free alkylborane–imidazole and phosphonium phosphate ionic liquids. They reported that phosphate tribofilms from phosphonium-phosphate IL exhibit better tribological properties than fluoride based tribofilms from halogenated IL. Recently, Qu et al.^{4, 32, 33} studied oil miscible phosphonium-

phosphate ionic liquids (PP-IL) as lubricant additives in base oil as well as in fully formulated oil. They reported comparable or even superior antiwear and anti-scuffing properties of phosphonium IL in comparison with the conventional additive i.e. ZDDP in PAO base oils at 0.1% Phosphorous.

In this study, six different ionic liquids were assessed in blends of group I mineral base oil on a cylinder on reciprocating flat tribometer. All oil formulations containing only IL were prepared at fixed 1000 ppm phosphorous (P) level. Morphology and surface topography of worn surfaces were studied using high resolution microscopy such as scanning electron microscopy (SEM) and scanning probe microscopy (SPM). The chemical nature of the tribofilms was explored using advanced surface characterization technique such as x-ray absorption near edge structure spectroscopy (XANES). ZDDP in base oil at 0.1 wt. % P and base oil only tests were also run for baseline comparison. Ionic liquids show comparable or improved wear protection on the rubbed surfaces in comparison to ZDDP at equal phosphorous levels.

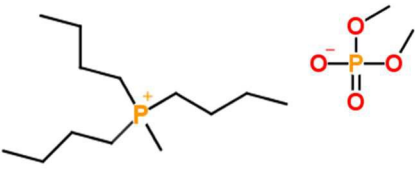
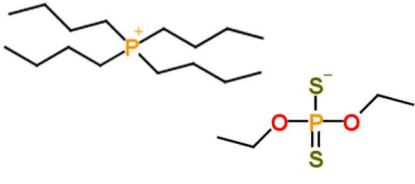
2. EXPERIMENTAL SECTION

2.1. Description of additive chemistry. Group I base oil (mixture of 60 wt. % solvent neutral 150W and 40 wt. % bright stock 90W) and zinc dialkyl dithiophosphate (ZDDP) were purchased from commercial vendors. The ZDDP used in this study is a secondary alcohol derived ZDDP with approximately 70% neutral and 30% basic characteristic. Six different ionic liquids studied were provided from AC²T Research GmbH Austria. Table 1 details the chemical structure of the antiwear additives used including ZDDP and the six ionic liquids. The six IL's were chosen carefully to provide not just a diversity of chemistries but also an opportunity to examine the role of different cations and anions. Choline bis(2-ethylhexy)-phosphate (N_DEHP) and choline dibutyl-dithiophosphate (N_DBDTP) have the same cation while one anion has phosphate structure and the other one has a thiophosphate structure. Tetradecyl-trihexyl-phosphonium bis(2,3,4-trimethylpentyl)-phosphinate (P_TMPP) and tetradecyl-trihexyl-phosphonium bis(trifluoroethylsulfonyl)-imide (P_TFSI) have the same cation while one anion is a phosphinate

the other one is a fluoro-sulfonyl amide. Lastly methyl-tributyl-phosphonium dimethyl-phosphate (P_DMP) and tetrabutyl-phosphonium O,O-diethyl-diphosphate (P_DEDTP) have similar (not same) cations while the anions have either a phosphate or thiophosphate moiety.

Table 1. Molecular structure of six IL's and ZDDP and their onset decomposition temperature.

Coded name	Chemical name	Chemical structure	Onset decomposition temperature (°C)
ZDDP	Zinc dialkyl-dithiophosphate (R = C4, C6 and C8)		206
N_DEHP	Choline bis(2-ethylhexyl)-phosphate		258
N_DBDTP	Choline dibutyl-dithiophosphate		172
P_TMPP	Tetradecyl-trihexyl-phosphonium bis(2,4,4-trimethylpentyl)-phosphinate		362
P_TFSI	Tetradecyl-trihexyl-phosphonium bis(trifluoromethylsulfonyl)-imide		413

P_DMP	Methyl-tributyl-phosphonium dimethyl-phosphate		326
P_DEDTP	Tetrabutyl-phosphonium O,O-diethyl-dithiophosphate		261

2.2. Thermogravimetric analysis of additives. Thermogravimetric analysis (TGA) of the ionic liquids was performed using Shimadzu TGA-51 Thermogravimetric analyzer. TGA was performed in nitrogen (N₂) atmosphere at a heating rate of 10 °C/min from RT to 600 °C with a N₂ flow rate of 20 mL/min. Each test was repeated twice for the consistency of the data.

2.3. Tribological test procedure. Oils containing ionic liquids were formulated in group 1 mineral base oil at 1000 ppm phosphorous level. Ionic liquids were mixed in base oil by pulse ultrasonication for 15 minutes in DI water bath. Tribological tests were carried out for each oil formulation immediately after the mixing. The tribological performance of these IL formulated oils were tested using a cylinder on reciprocating flat tribometer at Argonne National Laboratory³⁴. Friction and wear performance of IL's are compared with ZDDP at equal phosphorous level (i.e. 0.1 wt% P). Load was applied using a pneumatic pressure unit and friction forces were measured using a strain gauge motion sensor. Oil formulations containing IL's in base oil were tested under this set-up at 134 N applied load that generates a 500 MPa initial Hertzian contact pressure. All the test were run at 300 RPM (5 Hz) in pure sliding contact for the duration of an hour at 100 °C. Data was acquired at 5 Hz using the DasyLab software. Tests were performed on 52100 hardened steel flat using a 52100 hardened steel bearing cylinder from RBC bearings. Both flat and cylinder pin were cleaned before each tests using Stoddard solution followed by isopropanol and acetone to completely remove any oil and dust present on the initial surfaces.

The rubbed surfaces after the tests were cleaned with heptane and isopropanol and then saved by submerging in sulfur free base oil.

2.4. Tribofilms characterization methods. In order to make a precise measurement of average wear width, cylinders after each test were gently cleaned using heptane followed by isopropanol shower. Wear width were measured at nine locations on each cylinders using optical images obtained from an Olympus metallographic microscopy. The nature of the wear occurring at the surface was studied by examining the surface of the wear tracks using a Hitachi S-3000N SEM to obtain secondary electron images of the wear track and high resolution 3D images of the wear track were acquired using a nano-indentation from Hysitron Triboscope™ in SPM mode.

Tribochemistry of the films generated on the rubbing surfaces using IL's and ZDDP were characterized using XANES spectroscopy. It provides chemical information including local coordination of elements at different depths of penetration, for example in the case of phosphorous, surface can be probed from 5 nm to 60 nm in the case of P L-edge and from 50 nm of the surface to >800 nm in the case of P K-edge^{35, 36}. XANES spectra were obtained at The Canadian Light Source synchrotron facility at Saskatoon Canada. The phosphorous L-edge (P L-edge) data were collected at VLS-PGM (variable line spacing plane grating monochromator) beam station that operates at the energy range of 5.5 – 250 eV with a photon resolution of more than 10,000 E/ Δ E. All the spectra were collected using a 100 μ m x 100 μ m photon beam spot size. Oxygen K-edge (O K -edge) spectra were obtained at SGM (spherical grating monochromator) beam line that operates between 200 – 2500 eV energy range with a photon resolution of more than 5000 E/ Δ E. Here, a spot size of 50 μ m x 50 μ m was chosen to obtain high resolution spectra. Finally, phosphorous K-edge (P K-edge) and sulfur K-edge (S K-edge) spectra were obtained a SXRMB (Soft X-ray Microcharacterization Beamline) beam station which operates at higher energy from 1.7 – 10 keV with a photon resolution of 3.3×10^{-4}

Insb (111). A 1 mm x 2 mm spot size was chosen to collect the spectra at the SXRMB beam line.

Nano-mechanical properties i.e. hardness of the tribofilms generated on the flat were measured using a Hysitron TriboscopeTM. Nano-indentation tests were carried out using a NorthStarTM Cube Corner probe with a total included angle of 90° and <40 nm tip radius. Nano-indentation were performed at nine different locations in a single sample. A cyclic loading profile with partial unload load was run for each indentation point to study the nano-mechanical properties of the tribofilms as a function of film thickness.

3. RESULTS AND DISCUSSION

3.1. Thermogravimetric Analysis of Ionic Liquids. Figure 1 is a plot of weight loss as a function of temperature for six IL's and ZDDP antiwear additive. The onset of decomposition temperature for IL's and ZDDP additive was approximated using tangent analysis and is shown in Table 1. ZDDP additive showed onset decomposition temperature i.e. about 206 °C that is lower than IL's except N_DBDTP (i.e. 172 °C). N_DEHP was approximated to be about 258 °C whereas onset decomposition temperature of N_DBDTP was recorded to be about 172 °C. The P=O bond has a dissociation energy of 544 kJ/mole while P=S has a dissociation energy of 335 kJ/mole, hence it is easier for the P=S linkage to be the point of initial thermal decomposition in N_DBDTP leading to a lower decomposition temperature in comparison to N_DEHP. Similarly, N_DEDTP (P=S linkage) has lower onset decomposition temperature than P_DMP (P=O linkage). Choline based IL's exhibit lower thermal stability than phosphonium based IL structures with similar anions (N_DEHP vs. P_DMP and N_DBDTP vs. P_DEDTP). P_TFSI exhibited the highest thermal stability of all with onset decomposition temperature of about 413 °C.

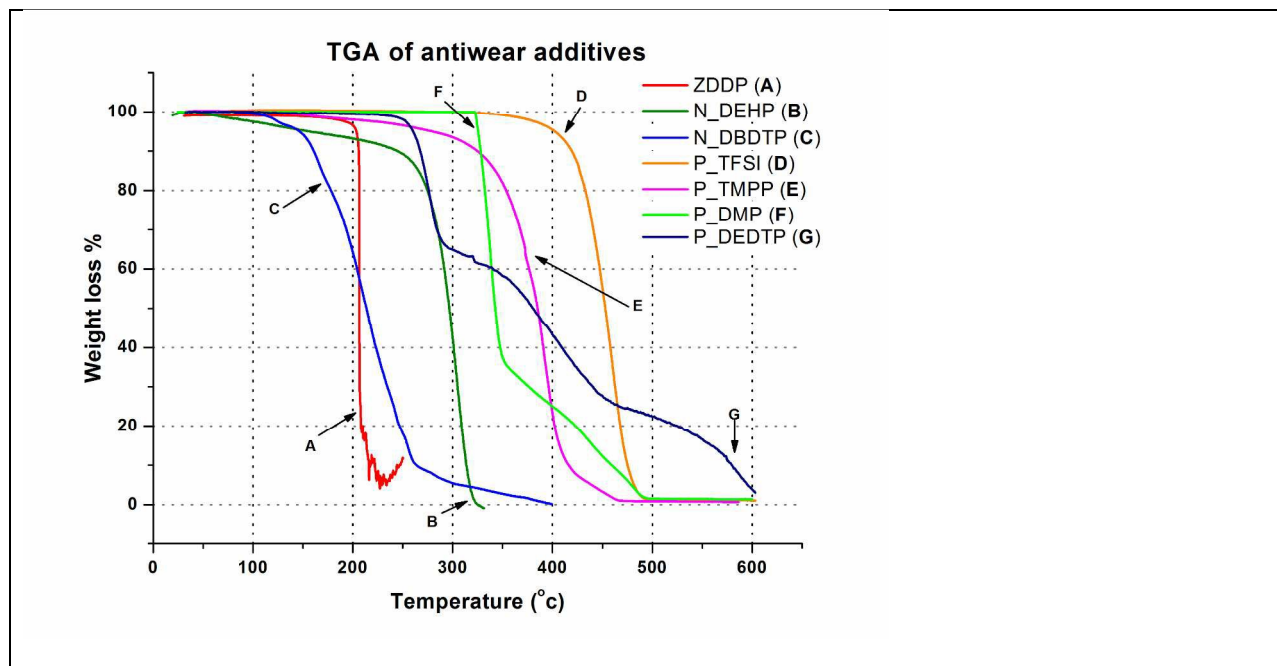
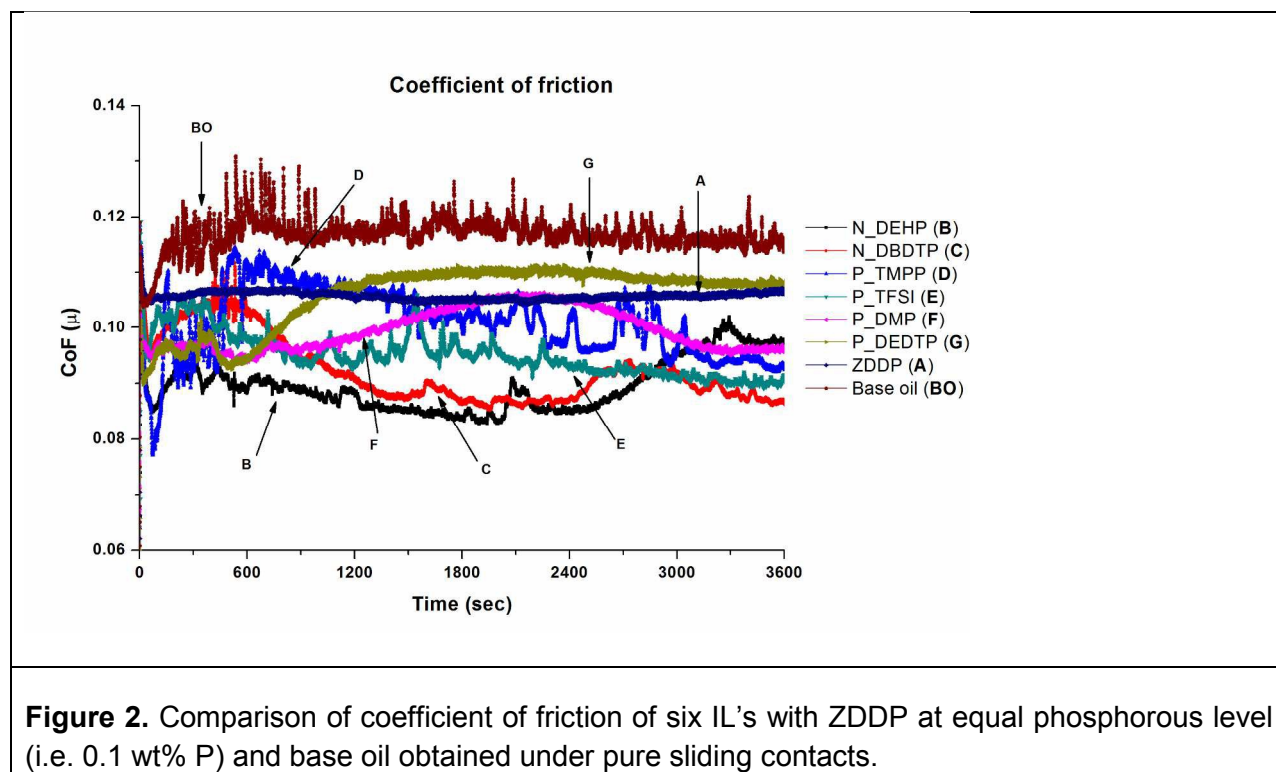


Figure 1. Thermogravimetric analysis plot of six IL's and ZDDP showing the decomposition temperature of different additive chemistries.

3.2. Evaluation of Coefficient of Friction (CoF) and Wear Volume. Figure 2 is a graph of friction coefficient as a function of the test duration for six ionic liquids and comparing their friction characteristic with ZDDP at equal phosphorous level as well as with group I base oil that has no additives. All six IL's and ZDDP show improvement in friction response compared to base oil when added at 0.1 wt% P treat rate. IL N_DEHP has the lowest friction coefficient however the CoF tends to increase at the end of the test. IL's N_DBDTP, P_DMP and P_TFSI also display lower friction coefficient in comparison to ZDDP for the duration of the test. On the other hand, ZDDP exhibits stable friction behavior throughout the test whereas all six IL's exhibit some level of variance in the friction with the progression of the test.



Wear was calculated by measuring the average wear width on the cylinder after each test using optical microscopy. Figure 3 is a plot of an average wear volume loss for six IL's along with ZDDP and base oil. In comparison with base oil, all IL's showed significant improvement in wear protection in base oil formulations. When compared with ZDDP, N_DEHP exhibited comparable antiwear performance whereas P_TFSI had slightly lower wear volume loss. On the other hand P_DBDTP, P_TMPP, P_DMP and P_DEDTTP exhibited significantly higher wear volume losses. Figure 4 summarizes tribological performances (i.e. CoF and wear volume loss) of six IL's along with ZDDP and base oil. Data at the bottom left on the plot has the lowest combination of wear and coefficient of friction (beneficial) and the data on the top right hand corner would have the higher wear and highest friction (detrimental). Hence, N_DEHP and P_TFSI have better tribological performance compared to ZDDP while P_DMP and P_DEDTTP have significantly worse wear but comparable frictional outcomes in comparison to ZDDP.

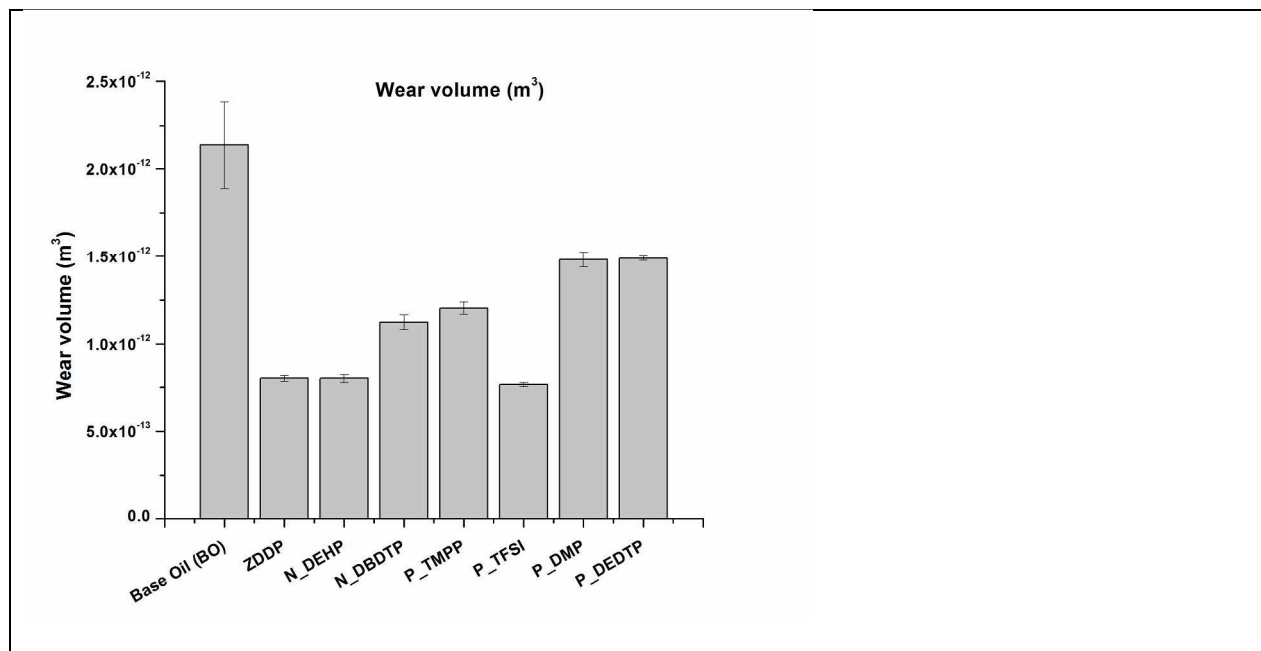


Figure 3. Average wear volume measured for six IL's and ZDDP blended in base oil at 0.1 wt% P and the neat base oil test.

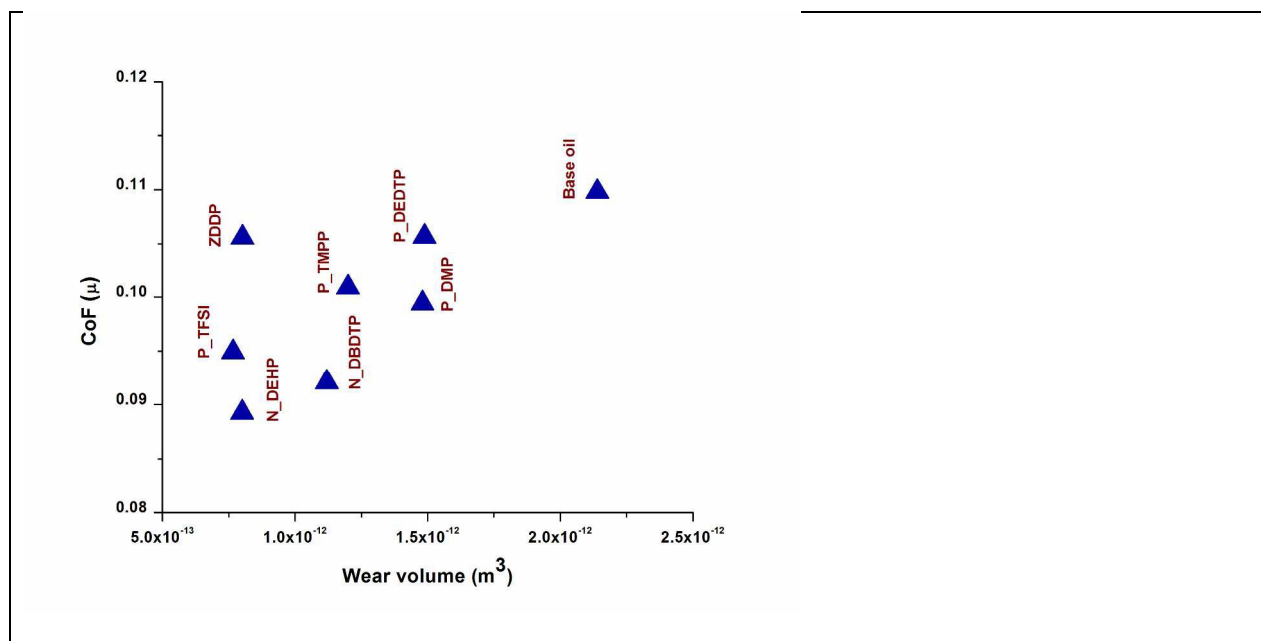
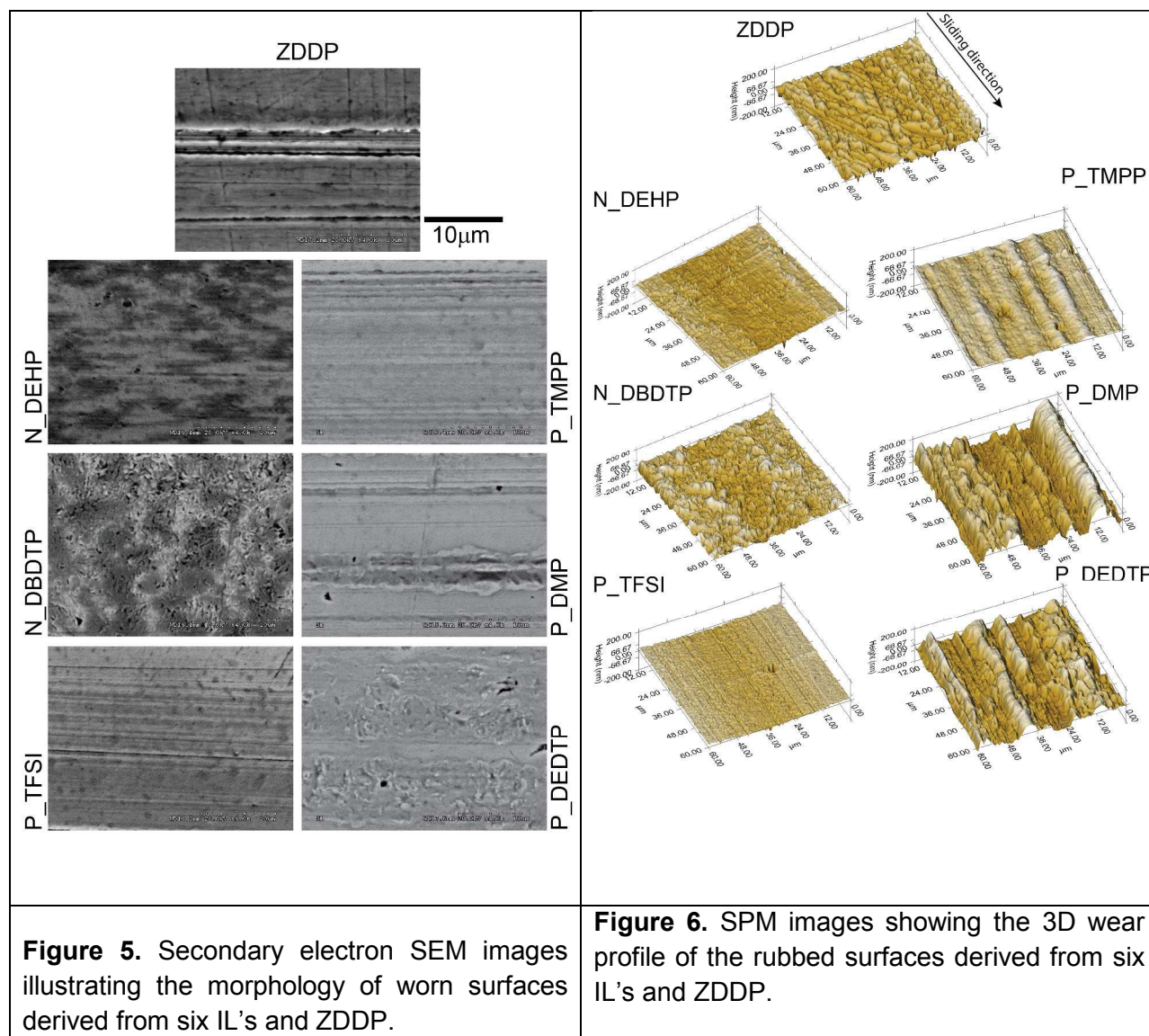


Figure 4. Comparison of coefficient of friction and wear volume loss for six IL's and ZDDP. Data at the bottom left on the plot has the lowest wear and friction coefficient (beneficial) and the data on the top right hand corner has the higher wear and highest friction (detrimental).

3.3. Analysis of Rubbed Surfaces Using Scanning Electron Microscopy and Scanning Probe Microscopy. Figure 5 is the secondary electron SEM images of the worn flat surfaces. SEM image of ZDDP lubricated surface exhibits regions of abrasive wear with scratches aligned to the sliding direction together with the formation of protective patchy tribofilms whereas worn surfaces lubricated under N_DEHP and P_TFSI show smoother wear surfaces. N_DEHP exhibits better coverage of tribofilms (as evidenced by the dark patches on the surface that are less conductive regions corresponding to patchy tribofilms) over the wear track with mild scratches aligned in the sliding direction. The SEM image obtained for P_TFSI lubricated wear track indicates mild polishing wear. The SEM image of N_DBDTP worn surface shows patchy tribofilm formation, with patch sizes that are larger than what is seen in N_DEHP. On the other hand the wear surfaces observed in the case of P_TMPP, P_DMP and P_DEDTP exhibit deeper scratches compared to N_DEHP, N_DBDTP and P_TFSI with P_DMP and P_DEDTP exhibiting the highest surface roughness. The analysis of the morphology of worn surfaces thus correlates to the wear volume discussed earlier as IL's P_TMPP, P_DMP and P_DEDTP had significantly higher wear volume whereas IL's N_DEHP and P_TFSI exhibited comparable or even better wear protection than ZDDP. In order to further compliment the findings of SEM results, SPM images were obtained using a nano-indentation technique in SPM imaging mode. SPM images of rubbed surfaces are obtained for 60 μm x 60 μm area on the wear track while keeping the Z-axis (± 200 nm) same. SPM images of IL's and ZDDP lubricated surfaces are shown in Figure 6. The arrow in Figure 6 represents the direction of rubbing. 3D wear profile of ZDDP lubricated surface exhibits slightly higher surface roughness with a number of small islands type features typical of patchy tribofilms covering the asperities whereas 3D profiles of N_DEHP and P_TFSI lubricated surfaces show smoother features on the wear track with smaller patches representative of tribofilms. SPM images of P_DEDTP, P_TMPP and P_DMP lubricated surfaces show scratches with larger peak to valley heights in the direction of rubbing

that complements the SEM results discussed earlier. The SPM images of N_DBDTP are slightly rougher than N_DEHP but smoother than P_DEDTP, P_TMPP and P_DMP.



3.4. Characterization of Tribofilms Using XANES. XANES spectroscopy is a non-destructive technique to characterize the chemical nature of tribosurfaces. XANES technique has a unique capability to provide information about the local coordination of elements present on the surface (5-50 nm) as well in the bulk of the sample (up to several hundred nm)³⁷. It utilizes a high flux of high-energy soft/hard x-ray photons from a synchrotron radiation source. If the flux of photons directed to the sample has sufficient energy to excite a core level electron of

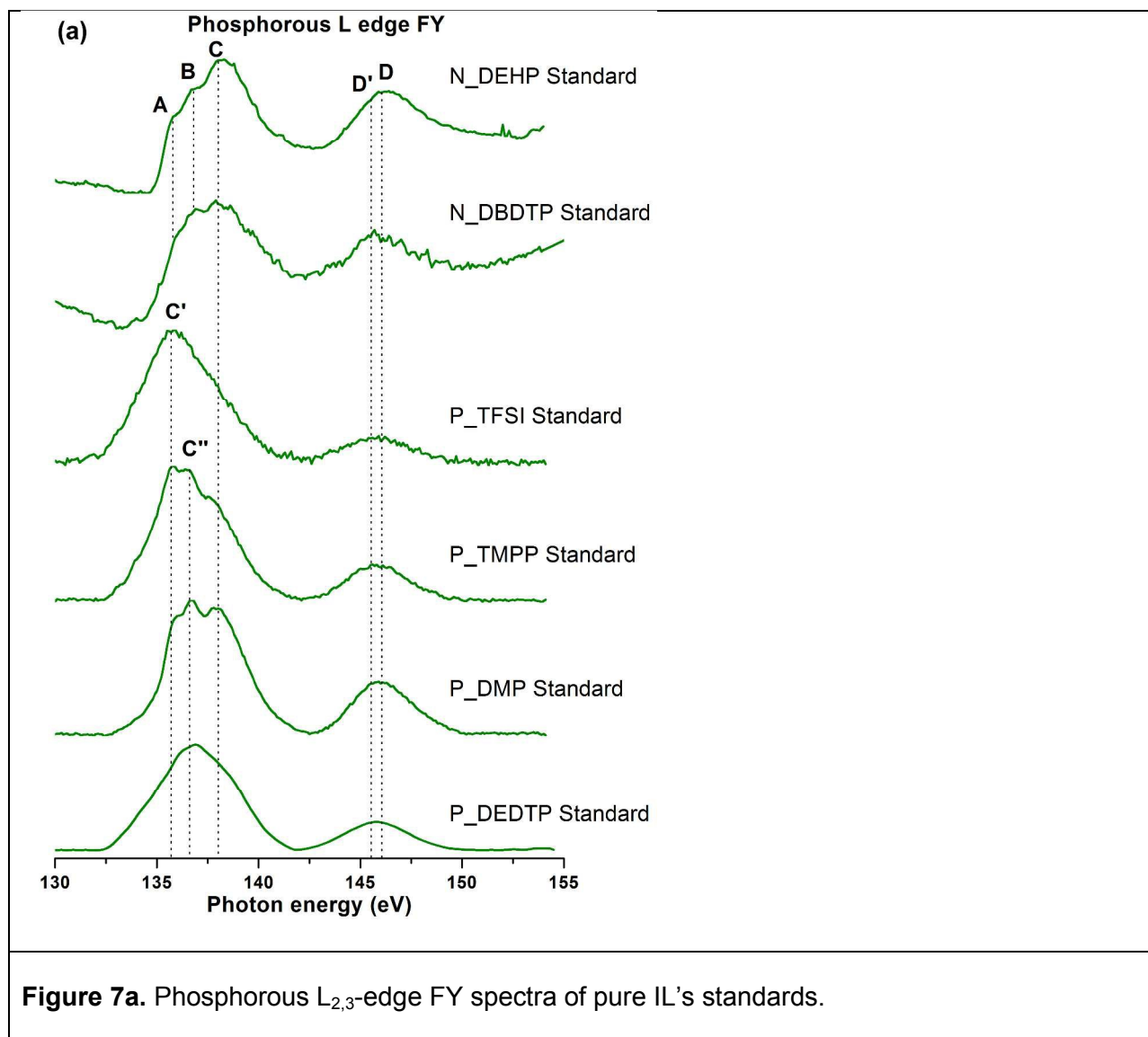
an atom, a photoelectron is created and it occupies unoccupied energy states. As a result, a hole is created in either K or L levels which subsequently gets filled up by electron from high energy shell followed by emission of a fluorescent photon which is detected by fluorescence detector inside the main chamber and plotted as fluorescence yield spectra (FY). Total electron yield spectra are collected by measuring a neutralization current that is applied to the sample to balance the positive charge created on the sample as X-ray photon absorption lead to the excitation of core level electrons to continuum. XANES spectra provide details about the electronic and geometric structure of the absorbing atom³⁸⁻⁴¹. In tribology, XANES analysis has been used extensively to examine the chemical composition of the tribofilms derived using various additives^{7, 9, 10, 12, 34, 36, 42-48}. In this study, XANES spectra are acquired in total electron yield (TEY) and fluorescence yield (FY) mode. TEY spectra is more surface sensitive whereas FY spectra give information from the bulk of the samples, in case of Si L-edge the sampling depth of TEY and FY mode is 5nm and up to 60 nm respectively³⁷.

3.4.1. Phosphorous L_{2,3}-edge of Pure IL's. P L-edge spectra of pure ionic liquid standards were also acquired in order to characterize the absorption edge of these novel compounds. To the author's best knowledge, this is a first paper that study and characterize the spectral features of a class of phosphorous based ionic liquids using P L_{2,3}-edge and P K-edge. Previously, Kruse et al.⁴⁹ have studied the P L-edge spectral features of a number of phosphorous compounds such as mineral P, organic P and P-bearing minerals. Similarly, Kasrai et al.^{43, 45, 50-52} studied the P L-edge and P K-edge spectral features of various sodium, iron and zinc polyphosphate glasses and proposed a relationship between the phosphate chain length and a peak ratio of pre-edge shoulder and main absorption edge. P L-edge spectra of pure IL standards is used to differentiate the chemical nature of the tribofilms formed using these novel additives from their respective original structures. P L-edge spectra of pure IL standards are shown in Figure 7a. The absorption peaks observed are labeled as **A**, **B**, **C**, **C'**, **C''**, **D** and **D'**. Where peak **D** is a shape resonance peak, which is a characteristic peak of

phosphate coordination irrespective of the cation it is associated with. Peak **D** is commonly present in IL's N_DEHP, P_TMPP and P_DMP, which have phosphate anion in their respective structures. The photon energy for peak **D** in Figure 7a is equivalent to the photon energy for peak **d** in Figure 7b, which is present in both FePO_4 and $\text{Zn}_3(\text{PO}_4)_2$ as well as in all the tribofilms composed of phosphate antiwear films. Main absorption edge for N_DEHP was observed at 138.09 eV (peak **C**), which is attributed to diethyl-hexyl-phosphate anionic moiety since here the only source of phosphorous is the cation. The absorption edge of N_DEHP IL is approximately 0.4 eV lower than the absorption edge for FePO_4 (138.06 eV for N_DEHP vs. 138.47 eV for FePO_4) as shown in Table 2. P L-edge spectra of N_DBDTP IL is similar to N_DEHP as their chemical structure is similar with the only difference being two of the four O atoms are replaced with S atoms in the phosphate. This is reflected in the P L-edge spectra where the shape resonance peak **D'** for N_DBDTP is slightly shifted to a lower energy compared to N_DEHP (peak **D**). P_TFSI spectra exhibit a main absorption edge (peak **C'**) at lower energy 135.79 eV compared to N_DEHP that is at 138.09 eV. This is attributed to the tetradecyl-trihexyl-phosphonium cation that is the only source of phosphorous in the P_TFSI structure, the shift to lower energy is likely due to the lower binding energy of the $2p$ electrons in organic moiety in the cation in comparison to the binding energy when P is bound to O in the anion. P L-edge spectra of P_TMPP and P_DMP IL's are quite rich as both IL's contain phosphorous in their respective cation and anion moieties. In the case of P_TMPP, peak **D'** originates from the trimethyl-pentyl-phosphinate anion whereas IL P_DMP show peak position **D** originating from dimethyl-phosphate. Besides that, multiple peaks are observed in the energy range between 135 eV - 140 eV. Presence of peak **C'** in both P_TMPP and P_DMP is attributed to the phosphonium cation (P-C coordination) in their respective spectra, which is also seen in the P_TFSI (peak **C'**) that only has phosphonium cation as a source of phosphorous in the structure. As seen earlier from N_DEHP, absorption edge peak **C** corresponds to the phosphate (P-O coordination) anion

structure that is also present in P_TMPP and P_DMP IL's. Peak **C''** is speculated to originate from the proximity of phosphonium cation and phosphate anion in P_TMPP and P_DMP, which is also present in P_DEDTP.

Table 2. P L-edge model compounds and Ionic liquids standard peak positions.									
Chemical compounds	Peak energy (eV)								
	A	B	C	D	E	a/a'	b/b'	c/c'	d
N_DEHP Standard	135.6	136.4	138.0		146				
N_DBDTP Standard		136.8	138.0	145.5					
P_TFSI Standard	135.7								
P_TMPP Standard	135.7	136.8			146				
P_DMP Standard	135.7	136.8	138.0		146				
P_DEDTP Standard		136.8		145.5					
Iron phosphate						135.8	136.7	138.4	146
Zinc Phosphate						136	137.9	138	146



3.4.2 Phosphorous $L_{2,3}$ -edge of Tribofilms. P L-edge TEY and FY spectra of the tribofilms generated under IL and ZDDP lubrication are plotted in Figure 7b and 7c respectively along with the model compounds. In Figure 7b and 7c, pre-edge shoulder and absorption edge for $Zn_3(PO_4)_2$ and $FePO_4$ are designated as a' , b' and c' and a , b and c respectively. Peaks labelled as a' , a and b' , b correspond to transition from spin-orbit split of phosphorous $2p$ electrons (the $2p_{3/2}$ and $2p_{1/2}$ levels, which are usually referred to as the L_{3-} and L_{2-} edges, respectively) into the first unoccupied $3s$ -like antibonding state⁵³. In $Zn_3(PO_4)_2$ and $FePO_4$ peaks labelled as c' and c are attributed to the transition of the phosphorous $2p$ electrons to the

3p-like antibonding state⁵³ in $Zn_3(PO_4)_2$ and $FePO_4$ respectively. Peak **d** in Figure 7b and 7c is commonly present in both $Zn_3(PO_4)_2$ and $FePO_4$ as well as in tribofilms spectra, is a shape resonance peak owing to *2p* to *3d* transition⁵⁴, which is a characteristic of all phosphates regardless of the structure. When comparing the tribofilms spectra with the model compound, P L-edge TEY and FY spectra from ZDDP tribofilm indicate the formation of zinc polyphosphates as the peaks **a'**, **b'** and **c'** from $Zn_3(PO_4)_2$ model compounds overlaps with the pre-edge shoulder and absorption edge of ZDDP tribofilms. However the possibility of formation of $FePO_4$ cannot be ruled out completely as iron cations are also available during the wear process. P L-edge spectra of IL's tribofilms show the presence of peak **d** suggesting that these novel antiwear additives undergo tribochemical reaction by decomposition of their original structure and form phosphate tribofilms during the rubbing action by reacting with counter surfaces. Since only iron cations are available from the substrate, these IL lubricated tribofilms are composed of iron polyphosphates, which can also be confirmed by matching the pre-edge shoulder (peaks **a** & **b**) and main absorption edge (peak **c**) of $FePO_4$ model compound with P L-edge spectra of IL's derived tribofilms in Figure 7b and 7c. XANES spectra can also be used to estimate relative thickness of antiwear films formed by considering the signal strength of their respective spectra. In case of P L-edge TEY spectra, all tribofilms spectra show good signal strength suggesting that tribosurfaces are enriched with phosphates films. Whereas P L-edge FY spectra that provide information from deeper in the tribofilm (up to 50 nm), a poorer signal to noise ratio can be seen in the case of P_TFSI and P_TMPP lubricated tribofilms suggesting thinner tribofilms.

P L-edge spectra can also be used to determine the chain length of the polyphosphates present in the tribofilms using peak intensity ratio of pre-edge shoulder (**a**) to main absorption edge (**c**). Chain lengths of polyphosphates are characterized on the basis of peak height of peak **a** relative to peak **c** where ratio **a/c** up to 0.3-0.4 represents short-chain polyphosphates and **a/c** > 0.6 indicates long-chain polyphosphates^{43, 45, 51}. The **a/c** ratio of tribofilms derived from IL's and ZDDP is shown in Table 3. From Table 3, it is apparent that tribofilms in this study

are primarily made up of short chain polyphosphates at the surface whereas the bulk of the tribofilms are composed of more medium chain polyphosphate films except N_DBDTP, P_DMP and P_DEDTP. Hence, a layered structure of tribofilms is observed with shorter chain at the top of the film and medium chain polyphosphate films in the bulk and close to the tribofilms substrate interface. Highest **a/c** or in other words longer chain polyphosphate films were observed in the case of N_DEHP, which earlier showed wear behavior comparable or better than ZDDP in Figure 3 & 4. P_TFSI that showed comparable or better antiwear outcome in comparison to ZDDP also have similar **a/c** ratio as of ZDDP tribofilms. In addition, N_DBDTP, P_DMP and P_DEDTP have lower **a/c** ratio and higher wear volume loss (Figure 3). Thus, it can be hypothesized that antiwear performance of these novel additive is a function of chain length of polyphosphate films formed under their respective lubrication. As an exception to this rule, P_TMPP formed medium chain polyphosphate tribofilm, however the signal to noise ratio is very poor. Here, it can be deduced that even though P_TMPP forms medium chain polyphosphates of iron on the rubbing surfaces, their film formation rate is a less competitive than film removal rate, which results in thinner protective phosphate films on the counter surfaces and consequently larger wear volume losses as seen in Figure 3.

Additive chemistry	TEY	FY
ZDDP	0.23	0.33
N_DEHP	0.24	0.49
N_DBDTP	0.33	0.21
P_TFSI	0.17	0.32
P_TMPP	0.2	0.45
P_DMP	0.22	0.16
P_DEDTP	0.23	0.17

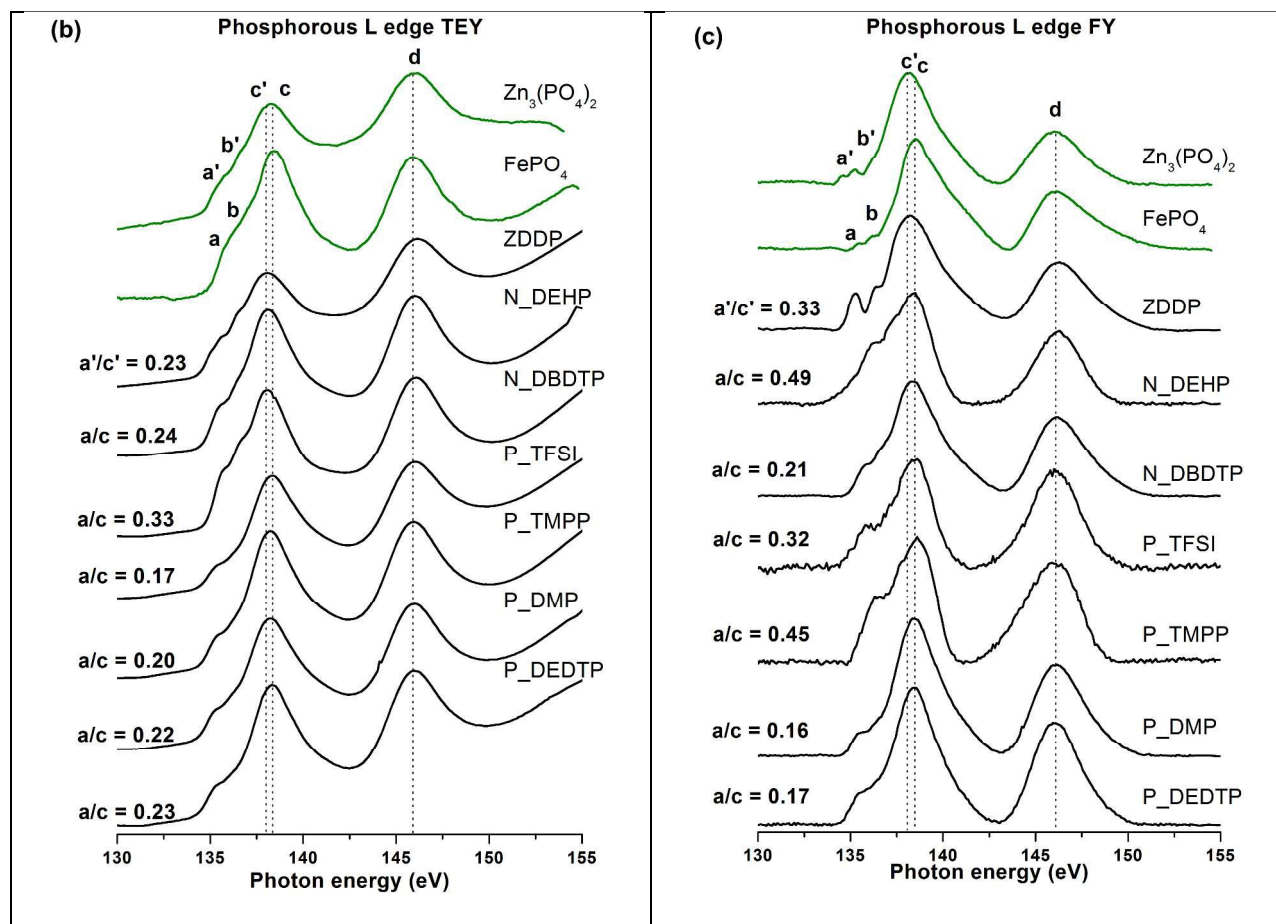


Figure 7. Phosphorous $L_{2,3}$ -edge spectra TEY (**Fig. 7b**) and FY (**Fig. 7c**) of tribofilms formed using ZDDP and six IL's additives. The a/c ratio obtained from P-Ledge indicating the degree of polymerization in the phosphate tribofilms is also shown in left hand side of each spectra.

3.4.3. Phosphorous K-edge of Pure IL's. In order to further consolidate the earlier findings that IL's do undergo a tribochemical reaction during the rubbing action, decompose and form tribofilms, P K-edge spectra of original IL structures are plotted in Figure 8a and compared with the P K-edge spectra of their respective tribofilms in Figure 8b. From Figure 8a and 8b, it can be seen that the main absorption edge of all six IL standards are at lower energy than the absorption edge of their respective tribofilms. Table 4 highlights the energy of the main absorption edge obtained for six IL standards as well as model compounds $Zn_3(PO_4)_2$ and $FePO_4$. From Figure 8a, a correlation between the chemical structure of IL's and their respective P K-edge spectra can be deduced. P K-edge spectra of N_DEHP exhibit main absorption edge

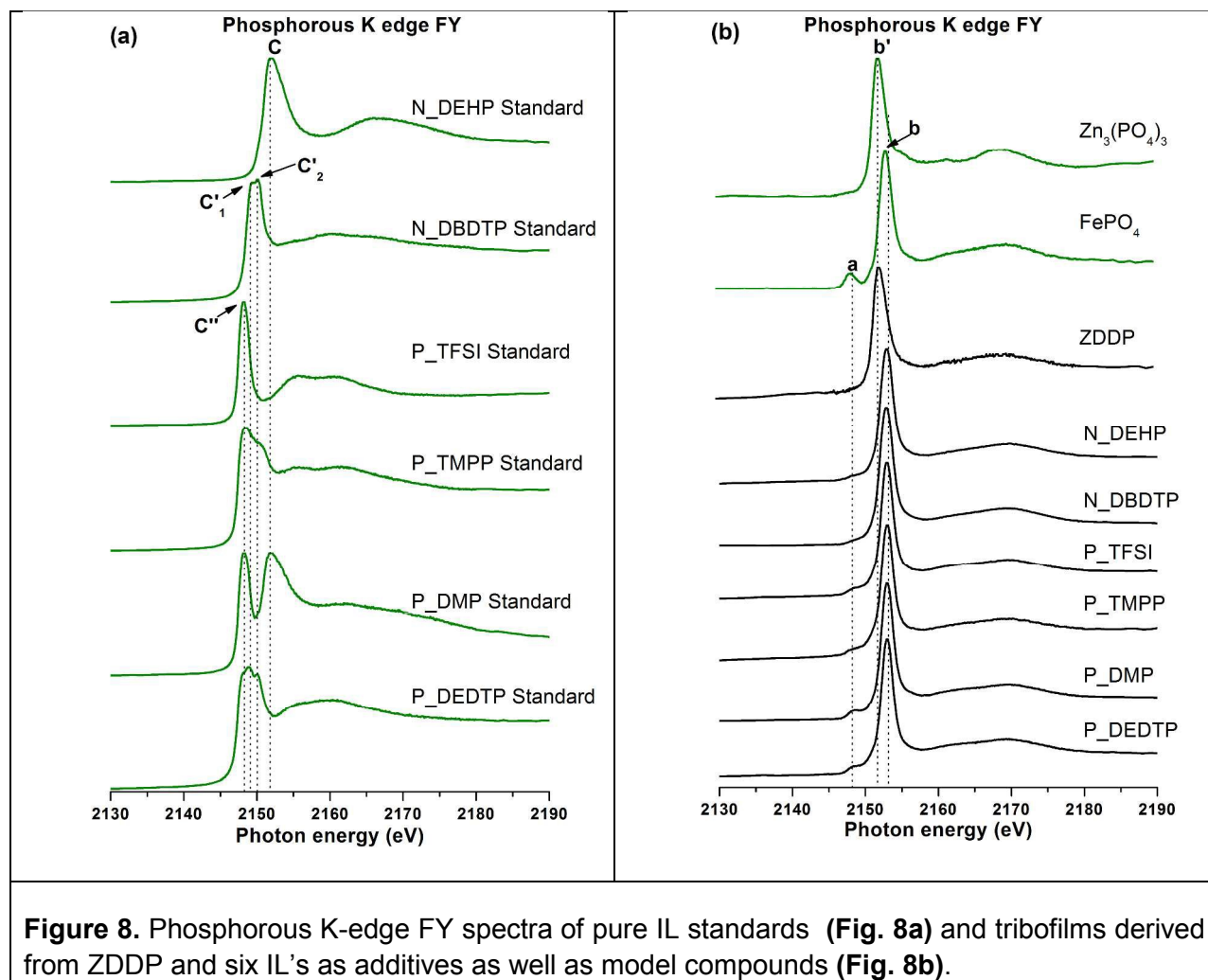
at photon energy 2151.8 eV that is identified as peak **C**. Peak **C** arises from the phosphate anion, since the only source of phosphorous in N_DEHP is (2-ethylhexyl)-phosphate anion. The absorption edge (peak **C**) for N_DEHP phosphate structure was found to be at slightly lower energy than the absorption edge energy of $Zn_3(PO_4)_2$ (peak **b'** in Figure 8b) as well as $FePO_4$ (peak **b** in Figure 8b) and N_DEHP derived tribofilms (peak **b** in Figure 8b) as the source of cation is different in all cases. Thus, the main absorption edge energy for these different phosphate structures can be ordered as $N_DEHP < Zn_3(PO_4)_2 < FePO_4 = N_DEHP$ tribofilm (Table 4). In the case of P_TFSI, phosphorous is only present in phosphonium cation (i.e. organo-phosphorous), and a respective absorption edge (peak **C''**) for P-C coordination was observed at 2148.2eV. N_DBDTP has the same cation as in N_DEHP but a different anion (i.e. dithiophosphate) where two O atoms are being replaced by two S atoms. The P K-edge FY spectra of N_DBDTP standard show two main absorption edges at energies of 2149.08 eV and 2150.05 eV and are identified as peaks **C'₁** and **C'₂** respectively. Peaks **C'₁** and **C'₂** are possibly originating from P-S & P-O coordination in dibutyl-dithiophosphate structure. We can further consolidate our findings by analyzing the P K-edge spectra of P_TMPP and P_DEDTP. P K-edge spectra of P_TMPP exhibit two main absorption edges since both cation and anion have phosphorous in their respective structure. The first absorption edge at energy 2148.25 eV aligns with the peak **C''**, which is originating from P-C coordination in tetradecyl-trihexyl-phosphonium cation. The second absorption edge in the P K-edge spectra of P_TMPP was found at energy 2150.1 eV matching with peak **C'₂**, which is believed to be originating from the phosphinate anion where phosphorous is bound with two O atoms as in the case of dithiophosphate anion in N_DBDTP. N_DEDTP has phosphorous both in cation and anion structure and its P K-edge spectra is more complicated as the absorption edge is influenced by three different phosphorous coordination i.e. P-C, P-S and P-O. Peak analysis using Origin pro identified three peaks in the main absorption edge of P_DEDTP P K-edge FY spectra. The main absorption

edge obtained at peak energy 2150.1 eV aligns with the peak C'_2 and is commonly found in N_DBDTP and P_TMPP with P-O coordination where one P atom is bound with two O atoms. The second absorption edge located at energy 2149.1 eV is found to match with the peak C'_1 that is also observed in N_DEDTP with P-S coordination where one P atoms is bound with two S atoms. And finally, a third peak identified at energy 2148.2 eV aligns with peak C'' is considered to be originating from P-C coordination in tetrabutyl-phosphonium. In the case of P_DMP, the first absorption edge (peak C') was observed at 2148.2eV originating from phosphonium cation and the second absorption edge was observed at 2151.86eV (i.e. peak C) originating from phosphate anion which is similar to the absorption edge observed in the case of N_DEHP with the similar phosphate anion structure. The main absorption edge (peak C'_2) observed in N_DEDTP for the P-O bond is found to be ~ 2.2 eV lower than peak C for the N_DEHP P K-edge. It is speculated that the partial replacement of O atoms by S atoms in dithiophosphate structure results in the change in the molecular symmetry and the local chemical environment of phosphate structure, leading to main absorption edge to be shifted at lower energy in N_DBDTP than N_DEHP for P-O binding.

Table 4. P K-edge model compounds and ionic liquids standard peak positions.

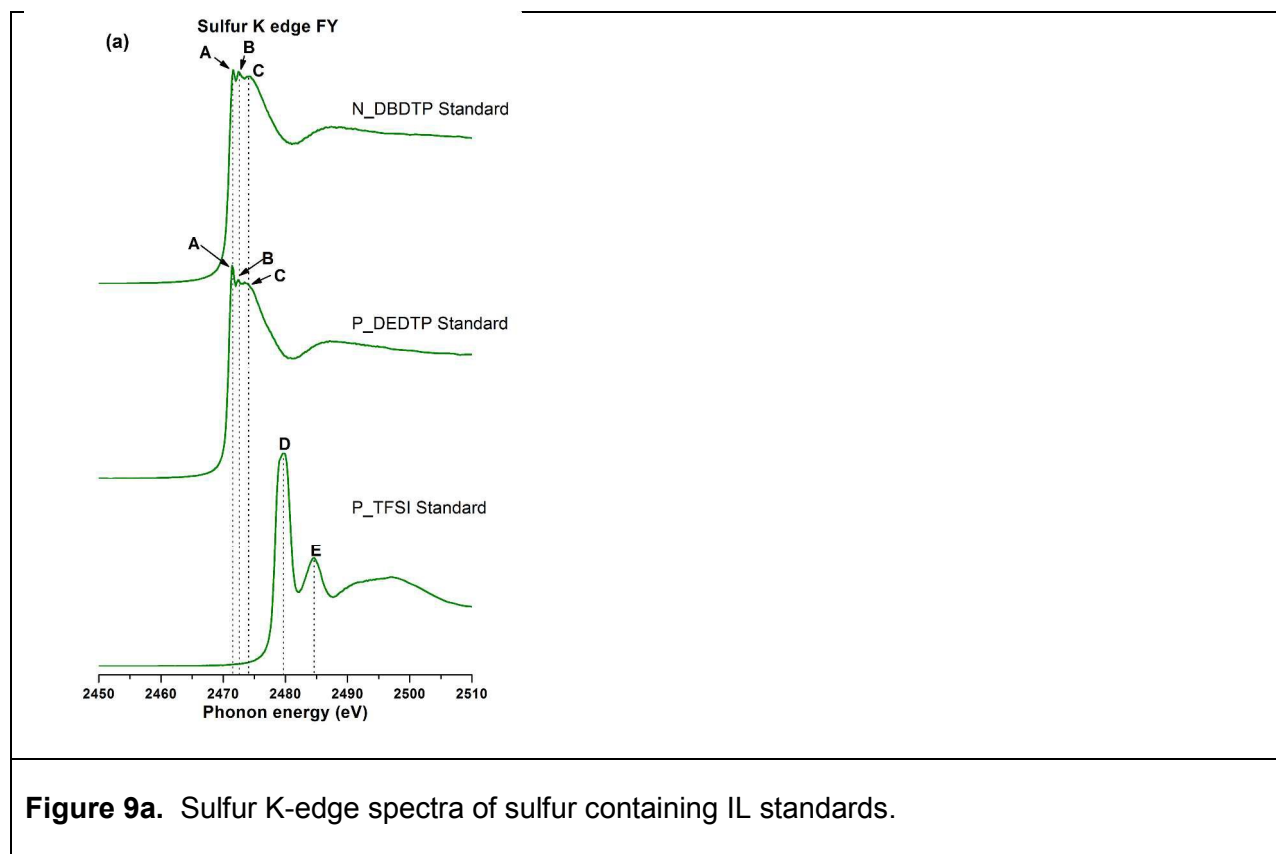
Model compounds	Peak energy (eV) (Figure 8a)				Peak energy (eV) (Figure8b)		
	C	C'_1	C'_2	C''	a	b	b'
N_DEHP Standard	2151.83						
N_DBDTP Standard		2149.08	2150.05				
P_TFSI Standard				2148.26			
P_TMPP Standard			2150.1	2148.25			
P_DMP Standard	2151.83			2148.25			
P_DEDTP Standard		2149.08	2150.05	2148.25			
Iron phosphate					2148.31	2153.22	
Zinc Phosphate							2152.2

3.4.4. Phosphorous K -edge of Tribofilms. Figure 8b is a plot of P K-edge FY spectra of tribofilms derived from ZDDP and six IL's used in this study. The P K-edge spectra of tribofilms are compared with model compounds $Zn_3(PO_4)_2$ and $FePO_4$ in Figure 8b. Primary absorption edge of $Zn_3(PO_4)_2$ is labelled as peak **b'** and a pre-edge shoulder and main absorption edge for $FePO_4$ are labeled as peak **a** and peak **b**. When spectra for $Zn_3(PO_4)_2$ and $FePO_4$ model compounds are compared, two main differences were evident, first the absorption edge for $Zn_3(PO_4)_2$ at peak **b'** (i.e. 2152.19 eV) is lower than the absorption edge for $FePO_4$ at peak **b** (i.e. 2153.22 eV), second, $FePO_4$ P K-edge spectra has a pre-edge shoulder at peak **a** (i.e. 2148.48 eV) that is absent in $Zn_3(PO_4)_2$. The information obtained from the P K-edge FY spectra of phosphate model compounds now can be used to do fingerprint match analysis of ZDDP and IL's tribofilms. P K-edge FY of ZDDP tribofilms show a main absorption edge matching with absorption edge of $Zn_3(PO_4)_2$ at peak **b'** suggesting that phosphorous in ZDDP tribofilms is mainly present in the form of zinc phosphate. P K-edge FY spectra of tribofilms derived from six IL's show two main features, a pre-edge shoulder at peak **a** and an absorption edge at peak **b** confirming that phosphorous from the P containing IL's contributes to the formation antiwear films composed of iron polyphosphate by interacting with the iron surfaces during the rubbing action. The spectra also clearly indicate that the tribofilms from IL are the result of decomposition of the IL and reaction of these decomposition products with the underlying iron substrate. No evidence of physically adsorbed IL on the surface of the tribofilm is present.



3.4.5. Sulfur K-edge of IL Standards and Tribofilms. Sulfur K-edge FY spectra of S containing IL standards (i.e. N_DBDTP, P_DEDTP and P_TFSI) are shown in Figure 9a. The main absorption edge and post edge shoulders identified from S containing IL's are labelled as **A**, **B**, **C**, **D** and **E** (in Figure 9a). Both N_DBDTP and P_DEDTP have S containing dithiophosphate anionic moiety with the only difference is in their respective alkyl group that is dibutyl in N_DBDTP and diethyl in N_DEDTP, therefore exhibit main absorption edge (peak **A** and peak **B**) and post edge shoulder (peak **C**) at the same photon energy. However, a fine difference can be seen as the relative intensity of peak **A** which is higher than peak **B** in the case of P_DEDTP whereas relative intensity of peak **A** and peak **B** is almost same in N_DBDTP. On the other hand, S K-edge spectra of P_TFSI standard with fluorosulfonyl-imide

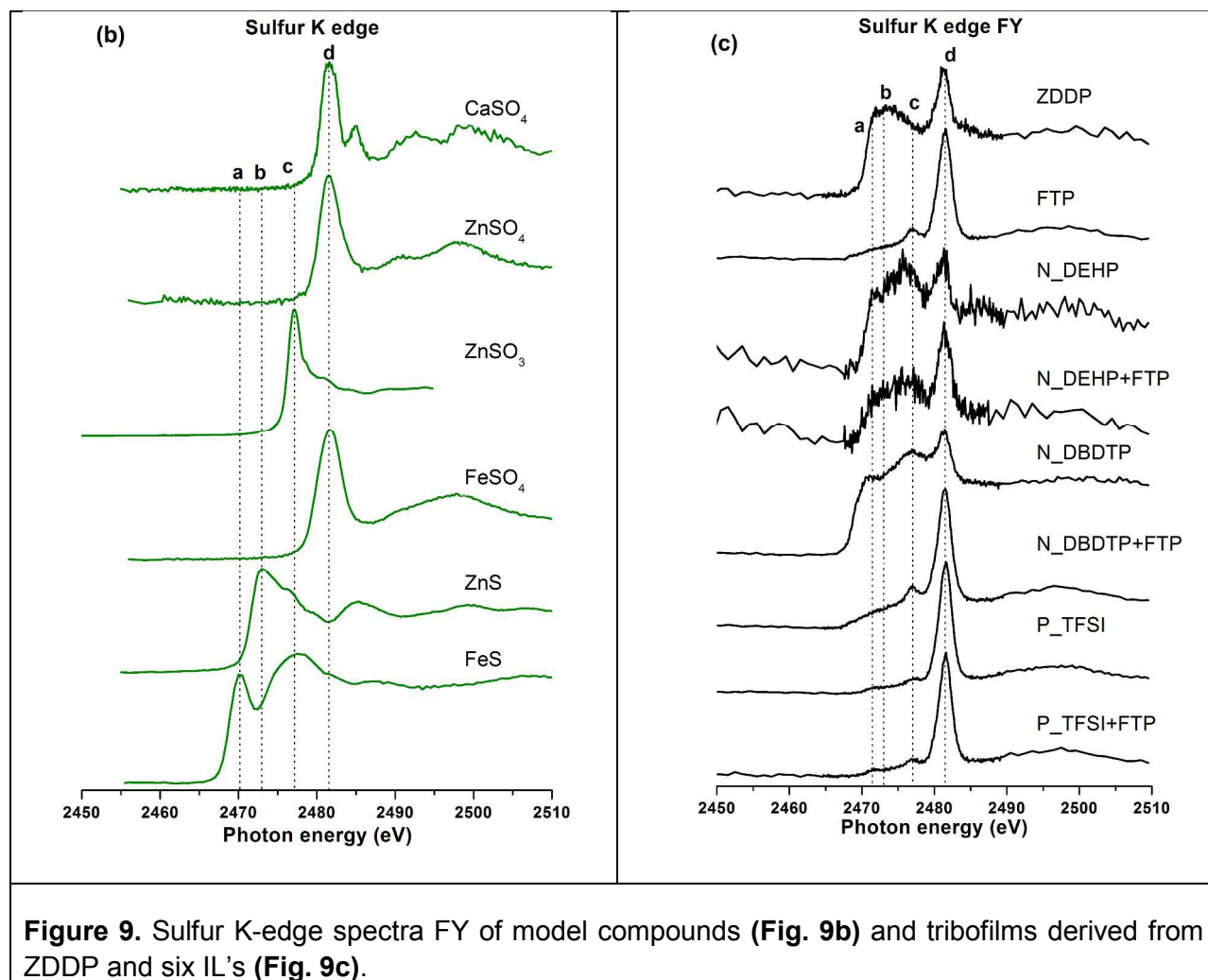
anionic moiety has a main absorption edge (peak **D**) and post edge shoulder (peak **E**) at higher energy than dithiophosphate containing IL's (N_DBDTP and P_DEDTP).



S K-edge spectra of tribofilms are plotted in Figure 9c and are compared with the model compounds in Figure 9b. Since sulfur exists in different valence states ranging from -2 to +6 with -2 being the reduced states and the +6 being the oxidized states various peaks have been identified in S K-edge model compounds spectra. The absorption edge identified from sulfur model compounds are labeled as **a**, **b**, **c**, **d** and **e** in Figure 9b. Where peak **a** and **c** corresponds to iron sulfide, peak **b** and **e** corresponds to zinc sulfide and peak **d** corresponds to sulfates and is characteristic of sulfate regardless of structures. Peak **e** also distinguishes calcium sulfate from zinc sulfate and iron sulfates. In Figure 9c, S K-edge FY spectra of ZDDP tribofilms primarily show two main absorption edge at peak **b** and peak **d** suggesting that sulfur in ZDDP tribofilms is primarily present in the form of ZnS (peak **b**) and sulfates (peak **d**) mainly ZnSO_4 as well as FeSO_4 to some extent. It can also be deduced from the spectra that sulfide to

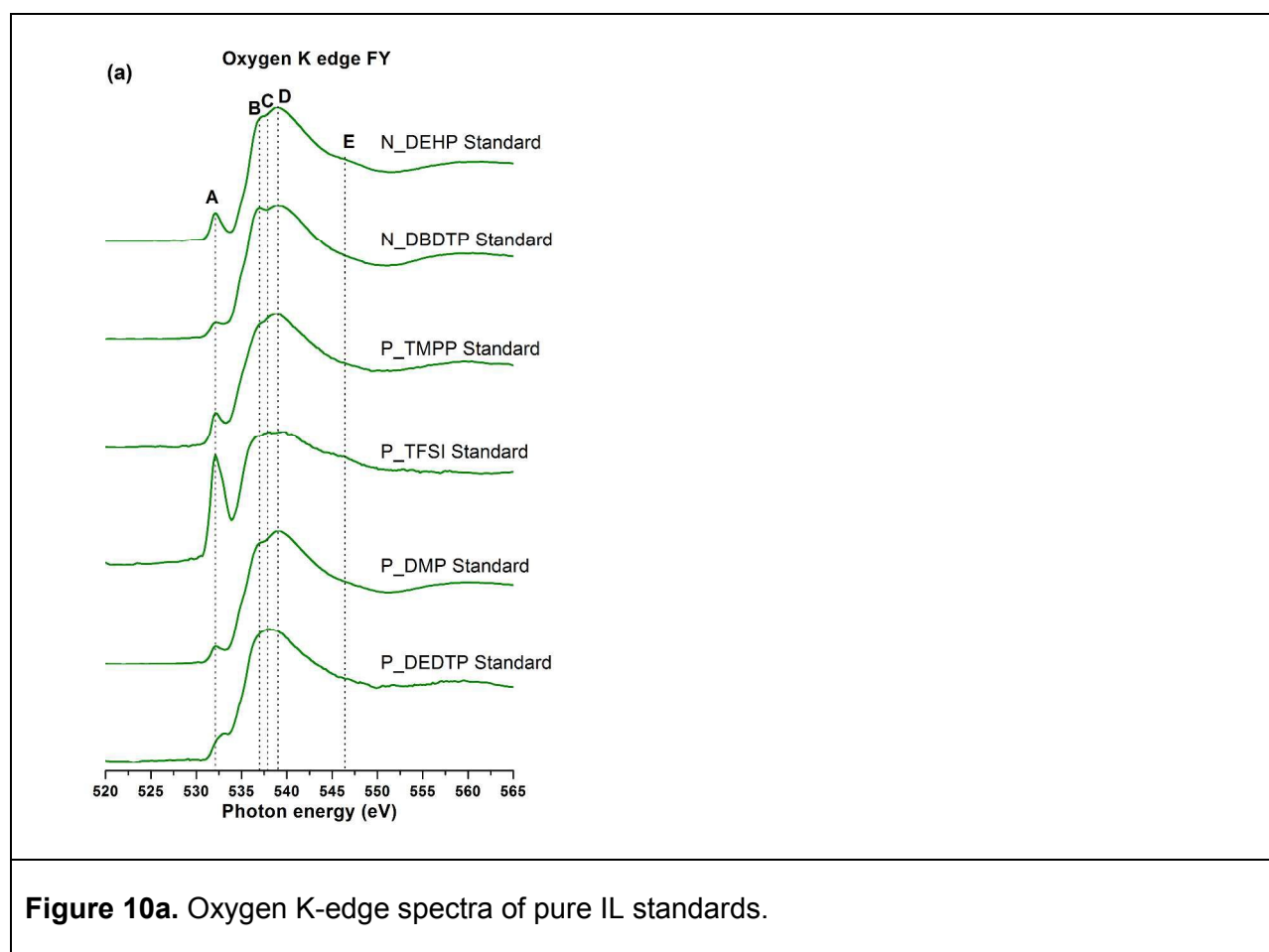
sulfate ratio is higher in ZDDP tribofilms. N_DEHP, P_TMPP and P_DMP do not have sulfur in the pristine structures yet their respective S K-edge tribofilm spectra exhibit a weak sulfur signal. The mineral base oil used in this study has sulfur impurity of about 300 ppm, which may provide a small amount of sulfur thus S K-edge spectra of N_DEHP, P_TMPP and P_DMP show weak sulfur signal confirming that there is not much sulfur present in their respective tribofilms. S K-edge FY spectra of N_DBDTP tribofilms feature peak **a**, **c** and **d** confirming the formation of FeS and FeSO₄ in the tribofilms. Relative intensity of sulfide peak to sulfate peak is higher in the case of N_DBDTP than the other sulfur containing IL's. P_TFSI and P_DEDTP also show strong signal for sulfates rather than sulfides in their respective S K-edge spectra.

S K-edge spectra can also be used to distinguish the state of sulfur in pristine IL standards and IL derived tribofilms. N_DBDTP and P_DEDTP derived tribofilms have main absorption edge at peak position **d** (2481.5 eV) in Figure 9c whereas the main absorption edge for pure N_DBDTP and P_DEDTP was found to be at lower energy i.e. peak **A** and peak **B** (2471.5 eV and 2472.5 eV) in Figure 9a suggesting that sulfur in the tribofilms is primarily present in the form of FeSO₄ instead of as in pure IL standard. In the case of P_TFSI, the main absorption edge of tribofilm was found at peak **d** (2481.5 eV) in Figure 9c whereas the main absorption edge of pure P_TFSI standard observed at peak **D** (2479.7 eV) and post-edge shoulder at peak **E** (2484.6 eV) in Figure 9a which suggest a change in the sulfur environment from the P_TFSI derived tribofilms to its respective chemistry in pure IL.



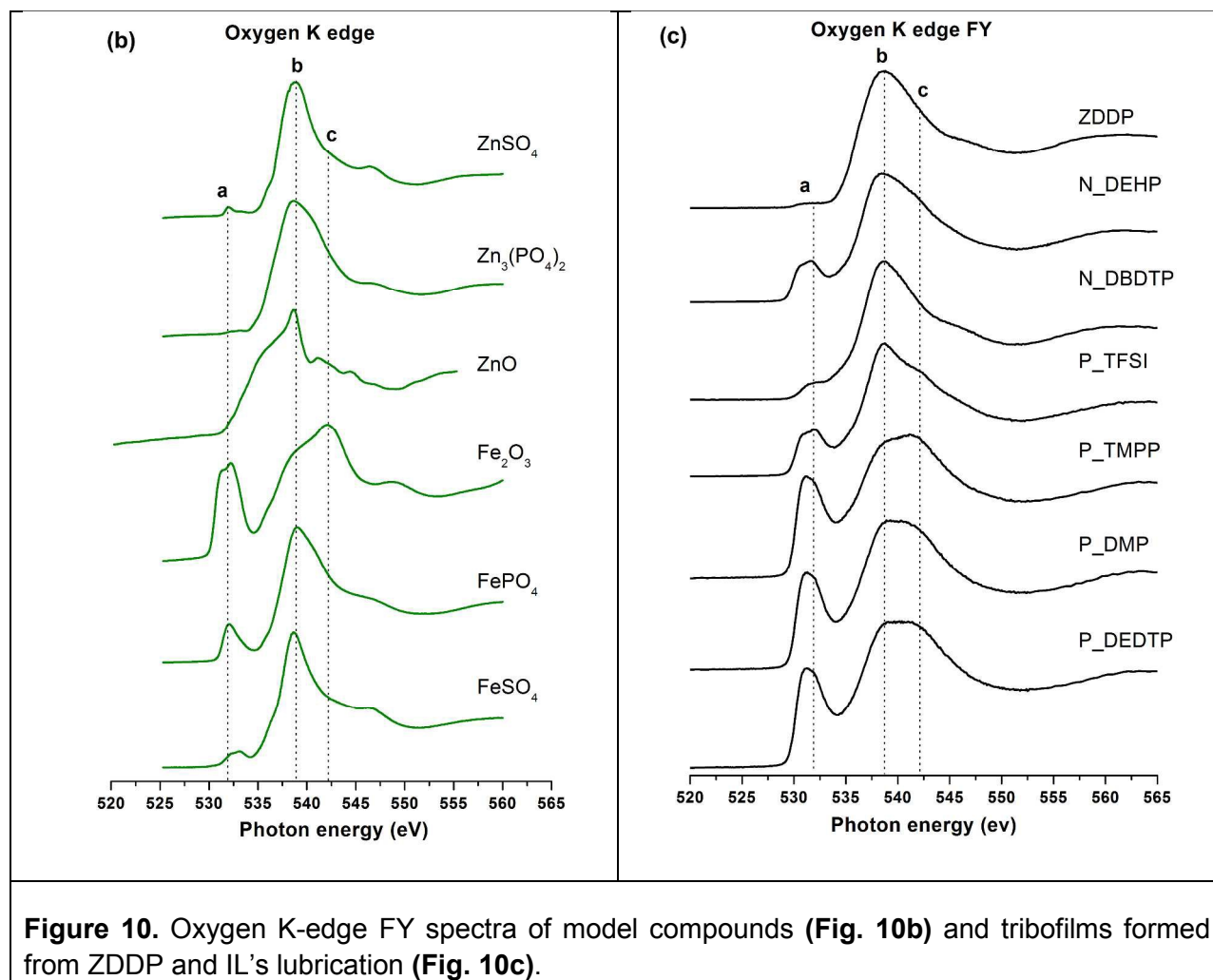
3.4.6. Oxygen K-edge of IL Standards and Tribofilms. Figure 10a illustrates the O K-edge spectra of six IL standards. The main absorption edge and the pre-edge and post-edge peaks are identified and labelled as peak **A**, **B**, **C**, **D**, and **E**. In all IL's except P_TFSI, oxygen has two linkage i.e. O bound with alkyl group (O-R linkage) and O bound with P atom (P-O linkage) while in the case of P_TFSI, O is only bound with S atoms. The oxygen K-edge spectra is more complex to resolve due to the superposition of multiple contributions at the main edge. However, all the model compounds except P_TFSI have P-O linkages that give rise to the pre-edge peak identified as **A**. This peak in the P_TFSI is accentuated, however, the likely origin of that large pre-edge is due to the O=S linkage. The main peaks located between 537-539 eV (**B**, **C**, and **D**) has contribution from multiple sources. Two absorption edge are observed for

N_DEHP at energy 537.8 eV i.e. peak **C** and 539 eV i.e. peak **D**. These two absorption edge are believed to originate from O-R and P-O linkage. Similar peaks are also observed in the case of P_DMP that has similar anion as in N_DEHP where four O atoms are bound with one P atom. When N_DEHP and N_DBDTP spectra are examined, peak **D** is diminished relative to peak **B** in N_DBDTP compared to N_DEHP. This possibly is because the four oxygen atoms in N_DEHP that are in P=O and P-O-C configuration and in N_DBDTP they are configured as P-O-C only.



O K-edge spectra of tribofilms are plotted in Figure 10c and compared with model compounds in Figure 10b. O K-edge spectra were acquired in both TEY and FY mode for the tribofilms and the model compounds as well as pure IL standards, TEY and FY spectra being very similar, only the FY spectra are shown for reference while the discussion pertains to both TEY and FY

spectra. Figure 10c is a plot for the O K-edge FY spectra of tribofilms derived from ZDDP and IL lubrication. Three peaks are identified and labeled as peak **a**, **b** & **c**. By fingerprint matching of these peaks with model compounds in spectra Figure 10b, it can be deduced that peak **a** is uniquely present in all the model compounds where oxygen is associated with Fe cation such as FePO_4 , FeSO_4 and Fe_2O_3 , peak **b** is a main absorption edge that is originating from either $(\text{PO}_4)^{-2}$ or $(\text{SO}_4)^{-2}$ structure whereas peak **c** is a main absorption edge for Fe_2O_3 model compound. O K-edge spectra of tribofilms generated using N_DEHP, N_DBDTP and P_TFSI show main absorption edge at peak **b** (538.9 eV) with a pre-edge peak at peak **a** (531.9 eV) whereas ZDDP tribofilms only show main absorption edge at peak **b**, suggesting the ZDDP tribofilms are primarily composed of $\text{Zn}_3(\text{PO}_4)_2$ and ZnSO_4 while the tribofilms derived from N_DEHP, N_DBDTP and P_TFSI are composed of FePO_4 in the case of N_DEHP and FePO_4 and FeSO_4 in the case of N_DBDTP and P_TFSI. A dominant presence of peak **c** (542.18 eV) in the case of tribofilms derived from P_TMPP, P_DMP and P_DEDTP indicate oxidation of the surfaces since peak **c** is characteristic absorption edge for Fe_2O_3 . This results from O K-edge spectra complements the wear results (seen in Figure 3) as IL's P_TMPP, P_DMP and P_DEDTP showed higher wear losses since the surface chemistry obtained using these IL's is being dominated by oxidation of the surfaces rather than formation of phosphate antiwear films. Whereas O K-edge spectra of additives with lower wear losses such as ZDDP, N_DEHP, P_TFSI show more phosphate formation on the rubbed surfaces rather than oxide formation.

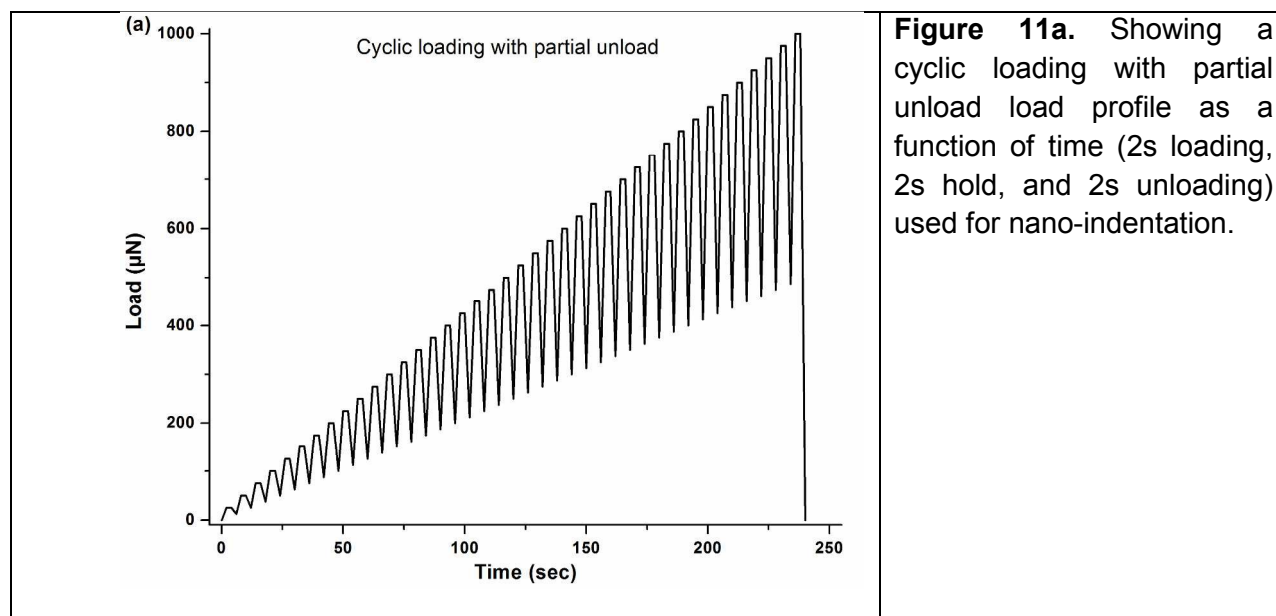


3.5. Nano-indentation. Since, XANES analysis revealed that the tribofilms derived from different additives such as ZDDP or IL's have different chemical make-up, it is important to understand the resultant mechanical properties of these different tribochemical films to evaluate their respective antiwear behavior. Nano-mechanical properties of tribofilms derived from IL lubricated surfaces were measured using nano-indentation technique. Hardness of IL derived tribofilms were compared with ZDDP lubricated tribofilms. Nano-indentation were performed on each tribofilms sample using a cyclic loading with partial unload function as shown in Figure 11a. Figure 11b shows a plot of tribofilm hardness as a function of film depth for ZDDP and IL's. Nano-mechanical properties of best antiwear performing IL's are compared with ZDDP in Figure 11b. In Figure 11b, top left graph shows a plot of applied vertical load against penetration depth

that is generated after each indentation test. Such typical load v/s depth plots were set as a criteria for the selection of proper indentation and hardness profile plotted for a particular indent location in the other three hardness plots. In the case of ZDDP, hardness profile varies with the indentation location, however, a general trend can be observed where ZDDP tribofilm hardness increases with the indentation depth up to 100nm and then remains constant. ZDDP tribofilms show large variation in hardness, where minimum hardness observed is ~3 GPa and maximum hardness is ~10GPa. Compared with ZDDP tribofilm hardness profile, both N_DEHP and P_TFSI show more consistent hardness profiles at different indentation locations suggesting that IL derived tribofilms have more uniform properties. N_DEHP tribofilms show low hardness at near surface and then hardness increases to peak value ~12 GPa at 40-50nm indentation depth and then starts to decrease with further depth as measurement gets influenced by substrate hardness (alloy steel) that has hardness ~8-10 GPa⁵⁵. P_TFSI show variation in hardness profiles at different locations but more than one location show similar hardness profiles suggesting that there are region of low hardness and high hardness. This could be explained as, in the case of peak to peak contact due to much higher contact pressure high hardness film forms whereas at regions of valley to valley contact remains relatively soft. Similarly, Bec et al.⁵⁶ also reported that pad regions (4 to 8 GPa) are harder than the valley region (1-3 GPa).

In all cases, surface of the tribofilms is softer than the bulk of the tribofilms with hardness increasing with indentation depth. This results are consistent with previous studies where similar hardness profile has been reported for the tribofilms. Nehme et al.⁵⁷ studied the effect of contact load on tribofilms properties and reported that ZDDP tribofilms hardness increase with indenter depth as well as with increasing contact pressure during the wear test. Furthermore, films hardness can also be correlated with the surface chemistry. P L--edge TEY spectra from XANES offer information up to 10-15 nm from the surface whereas FY gives information up to 50-60 nm. P L -edge a/c ratio calculated earlier in XANES analysis indicate that in the case of

ZDDP P L--edge a/c ratio increase from 0.23 (TEY) to 0.33 (FY) that subsequently results in increase in the ZDDP tribofilms hardness from 3 GPa to 8-9 GPa respectively (as seen in Figure 11a). Similarly, N_DEHP and P_TFSI have higher a/c ratio in FY spectra than TEY, which is an indicative of longer chain phosphates formation in the bulk of the films than the tribofilms at surface. From their respective hardness profile, it can be deduced that at the surface tribofilms with shorter chain phosphate have lower hardness (~3-4 GPa) and as the phosphate chain length increase the hardness of the films also increases (up to ~12 GPa). Highest hardness observed in the case of N_DEHP ~12 GPa that has highest a/c ratio of 0.49. This result is consistent with theoretical model developed by Mosey et al.⁵⁸ where they showed that longer chain lengths and crosslinking of zinc phosphate films resulted in higher stiffness tribofilms.



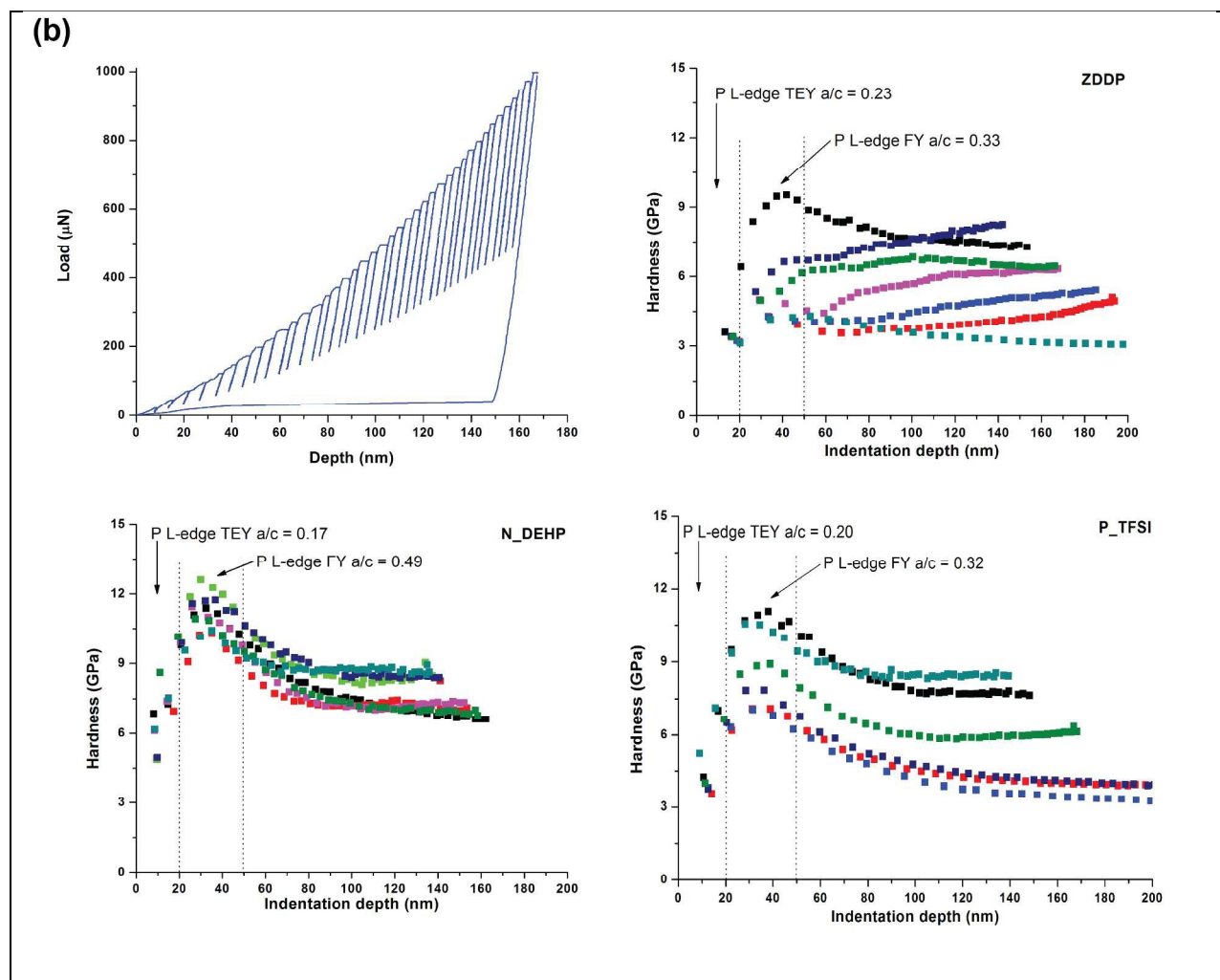


Figure 11b. Nano-mechanical properties of tribofilms obtained using a cube corner (NorthStar™) probe, a typical load vs. penetration depth curve obtained (shown in top left corner) set a criteria for proper indentation. Selected hardness profiles as a function of indentation depth are displayed for ZDDP (top right) and IL N_DEHP (bottom left), and P_TFSI (bottom right) tribofilms.

4. CONCLUSIONS

- Tribological properties of six IL's are studied and compared with ZDDP additive at equal phosphorous treat rate (i.e. 0.1 wt. % P) in group I BO. All IL's showed variance in their friction curve while ZDDP showed relatively consistent friction coefficient. Lowest CoF was recorded for IL N_DEHP. Both IL N_DEHP and P_TFSI showed comparable or even better wear protection than ZDDP whereas N_DBDTP, P_TMPP, P_DMP and P_DEDTTP showed worse wear outcomes than ZDDP.

- XANES analysis (P L_{2,3} & K-edge and S K-edge) indicate that tribofilms derived from IL lubricated surfaces have different chemical make-up than the original IL chemistry as the original structure of IL's are not found on the worn surface. Thus, it can be hypothesized that phosphorous containing IL's do participate in the tribochemical reaction during the rubbing action and form antiwear phosphate films on tribosurfaces under mixed to boundary lubrication conditions by interacting with Fe substrate. XANES analysis also showed that. These findings further lay out a strong understanding on the ability of IL's to interact with the rubbing surface and form glassy antiwear films composed of phosphates of Fe.
- P L-edge spectra of tribofilms showed that the surface of the tribofilms are composed of short chain polyphosphate and medium chain phosphates formed in the bulk except N_DBDTP, P_DMP and P_DEDTP.
- Nano-indentation results showed that N_DEHP derived tribofilms have uniform properties while ZDDP showed different hardness at different indentation location. In all cases, hardness increases from the surface towards the bulk.

5. Acknowledgments. XANES experiments were conducted at the Canadian Light Source, Saskatoon, Saskatchewan, Canada that is supported by NSERC, NRC, CIHR and the University of Saskatchewan. Tribological tests were performed at Argonne National Laboratory. Support provided by Dr. Ali Erdemir is gratefully acknowledged. Nano-indentation experiments were conducted at Center for Characterization for Materials and Biology at The University of Texas at Arlington. This work was also supported by the "Austrian COMET-Program" in the frame of K2 XTribology (project no. 849109).

- 1 K. Holmberg, P. Andersson and A. Erdemir, *Tribol. Int.*, 2012, **47**, 221-234 (DOI:<http://dx.doi.org/10.1016/j.triboint.2011.11.022>).
- 2 K. Holmberg, P. Andersson, N. Nylund, K. Mäkelä and A. Erdemir, *Tribol. Int.*, 2014, **78**, 94-114.
- 3 J. Qu, W. C. Barnhill, H. Luo, H. M. Meyer, D. N. Leonard, A. K. Landauer, B. Kheireddin, H. Gao, B. L. Papke and S. Dai, *Adv Mater*, 2015, .
- 4 J. Qu, H. Luo, M. Chi, C. Ma, P. J. Blau, S. Dai and M. B. Viola, *Tribol. Int.*, 2014, **71**, 88-97 (DOI:<http://dx.doi.org/10.1016/j.triboint.2013.11.010>).
- 5 V. Totolin, I. Minami, C. Gabler and N. Dörr, *Tribol. Int.*, 2013, **67**, 191-198 (DOI:<http://dx.doi.org/10.1016/j.triboint.2013.08.002>).
- 6 I. Minami, *Molecules*, 2009, **14**, 2286-2305.
- 7 V. Sharma, C. Gabler, N. Doerr and P. B. Aswath, *Tribol. Int.*, 2015, **92**, 353-364 (DOI:<http://dx.doi.org/10.1016/j.triboint.2015.07.009>).
- 8 J. Qu, P. J. Blau, S. Dai, H. Luo and H. M. Meyer III, *Tribology letters*, 2009, **35**, 181-189.
- 9 X. Chen, R. L. Eisenbaumer and P. B. Aswath, *Tribol. Int.*, 2013, **69**, 114-124.
- 10 X. Chen, B. Kim, R. Eisenbaumer, P. B. Aswath and P. B. Aswath, *Tribology - Materials, Surfaces and Interfaces*, 2012, **6(3)**, 121-133.
- 11 B. Kim, *Tribological Performance of Ashless Antiwear Additives Under Extreme Pressure Conditions*, University of Texas at Arlington, Arlington, Texas, 2009.
- 12 B. Kim, R. Mourhatch and P. B. Aswath, *Wear*, 2010, **268**, 579-591.
- 13 A. Erdemir and O. Eryilmaz, *Friction*, 2014, **2**, 140-155.
- 14 A. Ala'A, O. Eryilmaz, A. Erdemir and S. H. Kim, *Carbon*, 2014, **73**, 403-412.
- 15 V. Macián, B. Tormos, V. Bermúdez and L. Ramírez, *Tribol. Int.*, 2014, **79**, 132-139.
- 16 S. Keskin, D. Kayrak-Talay, U. Akman and Ö. Hortaçsu, *The Journal of Supercritical Fluids*, 2007, **43**, 150-180 (DOI:<http://dx.doi.org/10.1016/j.supflu.2007.05.013>).
- 17 J. S. Wilkes, *Journal of Molecular Catalysis A: Chemical*, 2004, **214**, 11-17 (DOI:<http://dx.doi.org/10.1016/j.molcata.2003.11.029>).
- 18 H. Zhao, *Chem. Eng. Commun.*, 2006, **193**, 1660-1677.
- 19 W. L. Hough and R. D. Rogers, *Bull. Chem. Soc. Jpn.*, 2007, **80**, 2262-2269.
- 20 T. Torimoto, T. Tsuda, K. Okazaki and S. Kuwabata, *Adv Mater*, 2010, **22**, 1196-1221.
- 21 C. Ye, W. Liu, Y. Chen and L. Yu, *Chemical Communications*, 2001, , 2244-2245.
- 22 W. C. Barnhill, J. Qu, H. Luo, H. M. Meyer III, C. Ma, M. Chi and B. L. Papke, *ACS applied materials & interfaces*, 2014, **6**, 22585-22593.
- 23 A. E. Jiménez, M. D. Bermúdez, P. Iglesias, F. J. Carrión and G. Martínez-Nicolás, *Wear*, 2006, **260**, 766-782 (DOI:<http://dx.doi.org/10.1016/j.wear.2005.04.016>).
- 24 H. Wang, Q. Lu, C. Ye, W. Liu and Z. Cui, *Wear*, 2004, **256**, 44-48.
- 25 M. Yao, M. Fan, Y. Liang, F. Zhou and Y. Xia, *Wear*, 2010, **268**, 67-71.
- 26 M. Cai, Y. Liang, M. Yao, Y. Xia, F. Zhou and W. Liu, *ACS applied materials & interfaces*, 2010, **2**, 870-876.
- 27 R. P. Swatloski, J. D. Holbrey and R. D. Rogers, *Green Chem.*, 2003, **5**, 361-363.
- 28 A. Jimenez and M. Bermúdez, *Tribology Letters*, 2007, **26**, 53-60.
- 29 L. Pisarova, C. Gabler, N. Dörr, E. Pittenauer and G. Allmaier, *Tribol. Int.*, 2012, **46**, 73-83 (DOI:<http://dx.doi.org/10.1016/j.triboint.2011.03.014>).
- 30 L. Pisarova, V. Totolin, C. Gabler, N. Dörr, E. Pittenauer, G. Allmaier and I. Minami, *Tribol. Int.*, 2013, **65**, 13-27.
- 31 V. Totolin, I. Minami, C. Gabler, J. Brenner and N. Dörr, *Tribology Letters*, 2014, **53**, 421-432.
- 32 J. Qu, D. G. Bansal, B. Yu, J. Y. Howe, H. Luo, S. Dai, H. Li, P. J. Blau, B. G. Bunting and G. Mordukhovich, *ACS applied materials & interfaces*, 2012, **4**, 997-1002.

- 33 B. Yu, D. G. Bansal, J. Qu, X. Sun, H. Luo, S. Dai, P. J. Blau, B. G. Bunting, G. Mordukhovich and D. J. Smolenski, *Wear*, 2012, **289**, 58-64.
- 34 V. Sharma, A. Erdemir and P. B. Aswath, *Tribol. Int.*, 2015, **82**, 43-57.
- 35 M. S. Fuller, L. R. Fernandez, G. Massoumi, W. Lennard, M. Kasrai and G. Bancroft, *Tribology Letters*, 2000, **8**, 187-192.
- 36 M. Nicholls, M. N. Najman, Z. Zhang, M. Kasrai, P. R. Norton and P. U. P. A. Gilbert, *Canadian Journal of Chemistry*, 2007, **85**, 816-830.
- 37 M. Kasrai, W. N. Lennard, R. W. Brunner, G. M. Bancroft, J. A. Bardwell and K. H. Tan, *Appl. Surf. Sci.*, 1996, **99**, 303-312.
- 38 A. Bianconi, D. Koningsberger and R. Prins, *XANES Spectroscopy (DC Koningsberger & R. Prins, eds.)*. John Wiley & Sons, Inc., New York, NY (573-662), 1988, .
- 39 A. Meisel, G. Leonhardt, R. Szargan and E. Källne, *X-ray spectra and chemical binding*, Springer, 1989.
- 40 P. Behrens, *TrAC Trends in Analytical Chemistry*, 1992, **11**, 237-244.
- 41 P. Behrens, *TrAC Trends in Analytical Chemistry*, 1992, **11**, 218-222.
- 42 Y. Li, G. Pereira, A. Lachenwitzer, M. Kasrai and P. R. Norton, *Tribology Letters*, 2007, **27**, 245-253.
- 43 Y. Li, G. Pereira, M. Kasrai and P. R. Norton, *Tribology Letters*, 2007, **28**, 319-328.
- 44 M. A. Nicholls, T. Do, G. M. Bancroft, P. R. Norton, M. Kasrai, T. W. Capehart, Y. -. Cheng and T. Perry, *Tribology Letters*, 2003, **15(3)**, 241-248.
- 45 M. N. Najman, M. Kasrai, G. M. Bancroft, B. H. Frazer and G. DeStatio, *Tribol. Lett.*, 2004, **17(4)**, 811-822.
- 46 G. Pereira, D. Munoz-Paniagua, A. Lachenwitzer, M. Kasrai, P. R. Norton, T. W. Capehart, T. A. Perry and Y. Cheng, *Wear*, 2007, **262**, 461-470.
- 47 M. N. Najman, M. Kasrai and G. M. Bancroft, *Tribology Letters*, 2004, **17(2)**, 217-229.
- 48 M. Najman, M. Kasrai, G. Michael Bancroft and R. Davidson, *Tribology International*, 2006, **39**, 342-355.
- 49 J. Kruse, P. Leinweber, K. Eckhardt, F. Godlinski, Y. Hu and L. Zuin, *Journal of Synchrotron Radiation*, 2009, **16**, 247-259.
- 50 M. Kasrai, M. Puller, M. Scaini, Z. Yin, R. W. Brunner, G. M. Bancroft, M. E. Fleet, K. Fyfe and K. H. Tan, in *Tribology Series*, ed. D. Dowson, C.M. Taylor, T.H.C. Childs and G. Dalmaz, Elsevier, 1995, p. 659-669.
- 51 Z. Yin, M. Kasrai, G. M. Bancroft, K. H. Tan and X. Feng, *Phys. Rev. B*, 1995, **51**, 742-750.
- 52 M. A. Nicholls, P. R. Norton, G. M. Bancroft and B. H. Do, *Trbol Lett*, 2004, **17**, 205-216.
- 53 G. Harp, Z. Han and B. Tonner, *Journal of Vacuum Science & Technology A*, 1990, **8**, 2566-2569.
- 54 D. Li, G. M. Bancroft, M. Kasrai, M. E. Fleet, X. H. Feng and K. H. Tan, *Am. Mineral.*, 1994, **79**, 785-788.
- 55 R. Mourhatch and P. B. Aswath, *Tribol. Int.*, 2011, **44**, 201-210
(DOI:<http://dx.doi.org/10.1016/j.triboint.2010.10.035>).
- 56 S. Bec, A. Tonck, J. M. Georges, R. C. Coy, J. C. Bell and G. W. Roper, *Relationship between mechanical properties and structures of zinc dithiophosphate anti-wear films*, London, UK, 1999.
- 57 G. Nehme, R. Mourhatch and P. B. Aswath, *Wear*, 2010, **268 (9-10)**, 1-1147
(DOI:10.1016/j.wear.2010.01.001).
- 58 N. Mosey, T. Woo, M. Kasrai, P. Norton, G. Bancroft and M. Müser, *Tribology Letters*, 2006, **24**, 105-114.

Graphical abstract

